Univerzita Karlova v Praze
Matematicko-fyzikální fakulta

DIPLOMOVÁ PRÁCE

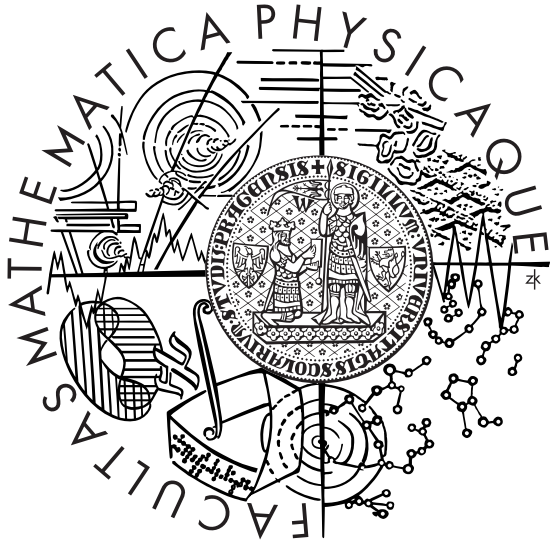

Tereza Brunátová

Studium nových typů nanotrubek Ti-NT, které lze použít jako plnivo do polymerní matrice

Katedra fyziky kondenzovaných látek

Vedoucí diplomové práce: doc. RNDr. Radomír Kužel, CSc.

Studijní program: Fyzika

Studijní obor: Fyzika kondenzovaných soustav a materiálů

Praha 2012

Charles University in Prague
Faculty of Mathematic and Physics

DIPLOMA THESIS

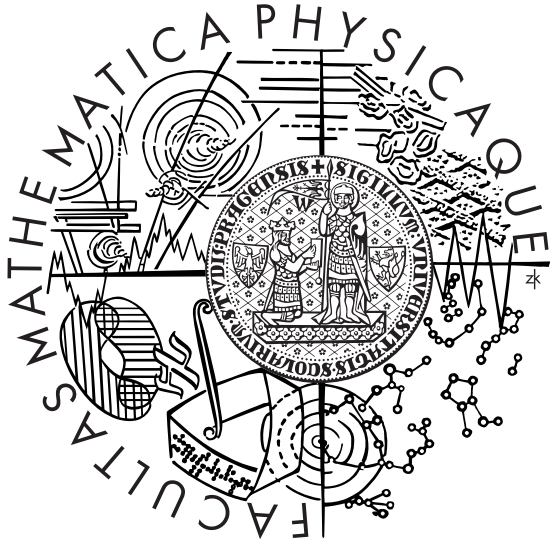

Tereza Brunátová

Study of new type of Ti-NT nanotubes that can be used as a filler in polymer matrix

Department of Condensed Matter Physics

Supervisor of diploma thesis: doc. RNDr. Radomír Kužel, CSc.

Study programme: Physics

Specialization: Physics of Condensed Matter and Materials

Prague 2012

Poděkování:

Ráda bych poděkovala svému školiteli
doc. RNDr. Radomíru Kuželovi, CSc. za vedení diplomové prace.

Poděkování rovněž náleží konzultantovi diplomové práce
doc. RNDr. Stanislavu Danišovi, Ph.D. za vytvoření zdrojových programů v jazyce C a za trpělivost při odpovídání na mé nekončící dotazy.

Za přípravu vzorků a pomoc s měřením snímků z transmisní elektronové mikroskopie bych chtěla poděkovat Ing. Daniele Popelkové z Ústavu makromolekulární chemie Akademie Věd ČR, v.v.i.

Za možnost zdokonalit svoje znalosti o transmisní elektronové mikroskopii a za možnost studovat v její skupině bych chtěla poděkovat profesorce Xiaodong Zou ze Stockholmské University a jejím spolupracovnikům: Peteru Oleynikovi, za pomoc s měrením a zpracováním dat z elektronové precesní difrakce, Weiovi Wanovi, za pomoc s měřením a zpracováním obrazů z transmisní elektronové mikroskopie s vysokým rozlišením a také profesoru Svenu Hovmöllerovi, za cenné rady.

Za pomoc s změřením snímků ze skenovací elektronové mikroskopie a změření energiově disperzní rengenové spektroskopie bych chtěla poděkovat Mgr. Alici Mantlíkové.

Dále bych chtěla poděkovat svým rodičům a přátelům, kteří měli se mnou trpělivost při vytváření této práce.

Tato práce vznikla za podpory těchto grantů: GAČR P108/11/1539 a část této práce vznikla v rámci studijního programu ERASMUS.

Prohlašuji, že jsem tuto diplomovou práci vypracovala samostatně a výhradně s použitím citovaných pramenů, literatury a dalších odborných zdrojů.

Beru na vědomí, že se na moji práci vztahují práva a povinnosti vyplývající ze zákona č. 121/2000 Sb., autorského zákona v platném znění, zejména skutečnost, že Univerzita Karlova v Praze má právo na uzavřen licenční smlouvy o užití této práce jako školního díla podle §60 odst. 1 autorského zákona.

V Praze dne 13.4.2012 Tereza Brunátová

Název práce: Studium nových typů nanotrubek Ti-NT, které lze použít jako plnivo do polymerní matrice
Autor: Tereza Brunátová
Katedra (ústav): Katedra fyziky kondenzovaných látek
Vedoucí diplomové práce: doc. RNDr. Radomír Kužel, CSc.

Abstrakt: Tato diplomová práce se snaží objasnit strukturu titanátových nanotrubek připravených pomocí hydrothermální syntézy TiO_2 prášku v roztoku NaOH. Struktura titanátových nanotrubek byla zkoumána pomocí dvou komplementárních metod - rentgenové difrakce a transmisní elektronové mikroskopie. Také byla studována změna struktury v závislosti na změně velikosti a krystalové struktury výchozího TiO_2 prášku. Byly vytvořeny tři různé modely pro dvě různé serie vzorků. Tyto modely byly následně použity pro výpočet práškového difrakčního záznamu, který byl následně porovnán se změřeným.

Klíčová slova: titanátové nanotrubky, počítačové simulace práškových rengenový difrakční záznamů, rengenová difrakce, elektronová mikroskopie

Title: Study of new type of Ti-NT nanotubes that can be used as a filler in polymer matrix
Author: Tereza Brunátová
Department: Department of Condensed Matter Physics
Supervisor: doc. RNDr. Radomír Kužel, CSc.

Abstract: The subject of presented work has been devoted to a structure of titanate nanotubes which were prepared by hydrothermal treatment of TiO_2 powder in NaOH solution. Structure determination was done mainly with two complementary methods - X-ray diffraction and transmision electron microscopy. A influence of structure by changing particle size and crystal structure of the initial powder TiO_2 was studied as well. Three different models of nanotube structure were build. These models were used for a calculation of powder X-ray diffraction pattern and they were compared to experiment pattern.

Keywords: titanates nanotubes, computer simulations of powder X-ray diffraction patterns, X-ray diffracion, electron microscopy

Contents

1. Introduction

Interest in nanotubular structure began after the first synthesis of carbon nanotube in 1991 made by Iijima [1]. Then chemists tried to prepare other inorganic nanotubular structures such as BN, SiO_2, Al_2O_3, V_2O_5 [2]. In 1998, an article on titanium dioxide nanotubes (titania or titanate - depends on the possible structure - nanotubes - Ti-NT) was published by Kasuga et al. [2]. A cheap and easy method of preparation of Ti-NT was described. This method is called hydrothermal treatment of TiO_2 powder in NaOH solution. Thanks to potential applications of Ti-NT for example in solar cells and photocatalysts, see section 1.2, big interest in these materials started. Unfotunately the structure of Ti-NT has not been clearly understood and the main aim of this diploma thesis was to found possible structure of Ti-NT prepared by hydrothermal method.

1.1. Titanium dioxide

Starting material for preparation of Ti-NT is titanium dioxide. TiO_2 is nontoxic semiconductor, nonsoluble in water, chemically stable. Generally it has white color. TiO_2 has three most common stable crystallographic phases: rutile, anatase and brookite. The thermodynamically most stable phase is rutile, the other two phases transform to rutile by heating. The phase transition from anatase to rutile occurs at about 700°C or lower depending on crystallite size and anatase preparation. TiO_2 powder is used in many applications - and it can even be used in daily life, some of them are listed below:

- pigment

  TiO_2 is the most known as a bright white pigment in many commercial applications: paints and coatings, plastic, paper, glass, porcelain, toothpastes, foods, medicines and cosmetics. For example, in toothpastes TiO_2 is used for whitening of teeth and for removing of dental plaque. Another example from food industry is adding TiO_2 to milk on purpose to have it more white. Chemical stability of TiO_2 is advantageous for food industry - titanium dioxide goes through the human body without changes [3], [4].

- sunscreens and UV absorber

  TiO_2 has one of the highest refractive indices and for its optical properties it is used in cosmetics as an UV absorber. It is resistant to ultraviolet light as well, thus it can be utilized in sunscreens. For sunscreens,

titanium dioxide is applied in the form of nanoparticles. The nanocrystals of TiO_2 are coated with silica to avoid realising the radical that are created during photocatalytical reaction.

- photocatalysis

  Photocatalytic activity is an ability of a material to create an electron-hole pair, the secondary reaction is creation of free radicals, which is possible when the catalyst react with water molecules [5].

  - ⁕ superhydrophilicity and self cleaning surface

    The TiO_2 in form of a thin layer on glass or mirrors displays superhydrophilic properties. On this surface, self cleaning reaction appears due to the strong oxidizing property of TiO_2 [5]. For example, self cleaning windows are already commercial available [6].

  - ⁕ If the TiO_2 is utilized as a special pigment on a top layer of walls color, it protects the color from UV light and self-cleans the wall by means of photocatalytical reaction.

  - ⁕ antibacterial, anti-viral, antifungicidal, air purification

    This area of utilization of TiO_2 starts to be very popular, because of application - cleaning the air. Special TiO_2 pains [7], sprays [8] or pictures [9] are commercionally available from several manufacturers. When irradiated by ordinary light or special UVA lamps, the photocatalytic reaction starts and destroys unhealthy organic microorganism and bad smell (anorganic unhealthy component in air) in a room. A special application has been found in clean hospital rooms [5].

  - ⁕ mosquito trap

    Surprisingly, TiO_2 can help to protect us from insects. For example, mosquitoes are sensitive to temperature and carbon dioxide. The commercionally available device is called mosquito trap. It works by capturing insects by giving them what they need. TiO_2 gives the necessary carbon dioxide by photocatalytic reaction, which starts by a fluorescent lamp. That gives also important heat. This device is commercial available [10]. The principle of this device is shown in Figure 1.1.

- dye-sensitized solar cell

  In dye-sensitized solar cell, TiO_2 is utilized as an nanocrystallic powder. In nano-sized powder, TiO_2 is conductive and it assists in the electron transport from dye (where the electrons are produced by solar light) to anode [11].

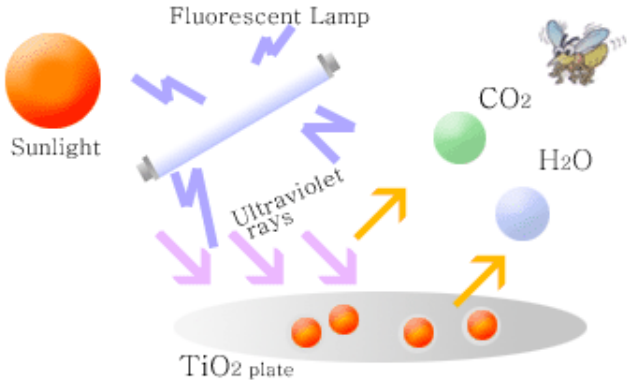

Figure 1.1: The photocatalytic reaction in mosquito trap [10].

1.2. Possible application of titania (titanate) nanotubes

Ti-NT have quite the same applications as a 'normal' TiO_2 powder, but their main advantages are the elongated structure and the high specific surface area. Some of possible application of Ti-NT are listed bellow:

- reaction catalyst

  For applications in catalysis, the high surface area and adaptation between catalyst and support are important. In order to obtain better catalytic properties, Ti-NT are doped by various metal atoms. The most studied catalyst is Au/Ti-NT which has demonstrated high activity for CO_2 reduction by hydrogen and water shift reactions. Another catalyst is Cu^{2+}/Ti-NT - it has good activity and selectivity for the catalytic reduction of NO. In addition Pt/Ti-NT has a good performance in the selective reduction of CO with H_2 to form CH_4 and in the water shift reaction (Bavykin and Walsh [12]).

- photocatalysis

  Titanium dioxide is widely used as a wide-band gap photocatalyst for the oxidation of organic compounds. The best TiO_2 based catalysts are characterized by a highly crystalline structure which reduces recombination of photogenerated carriers. The crystallinity implies a high specific surface area that provides acceleration of the interfacial reaction rate, and abundance of surface OH groups this is required for the generation of OH radicals during photocatalytic reactions. All these

features are found for Ti-NT as well. Crystallinity of Ti-NT can be improved by heating because they are transformed to nanowires.

The photocatalytic properties are strongly affected by Na atoms within the sample. If sodium ions are present in samples, mentioned photocatalyc quality decreases. Nanocrystalline structures based on TiO_2 have been considered for photocatalytic processes - oxidation of organic waste in air and water, splitting of water (demonstrated in Figure 1.2) and generation of hydrogen. Photocatalytically active TiO_2 has already been used to cover glass as self-cleaning surfaces, which, under UV light, gain antifogging and super-hydrophilic properties. The Ti-NT or Ti-nanorods(wires) have better surface wettability. In order to make Ti-NT sensitive also to visible light it is necessary to dope the structure with nitrogen or chromium ions. This adds levels in the forbidden zone of the wide-band-gap (Bavykin and Walsh [12]).

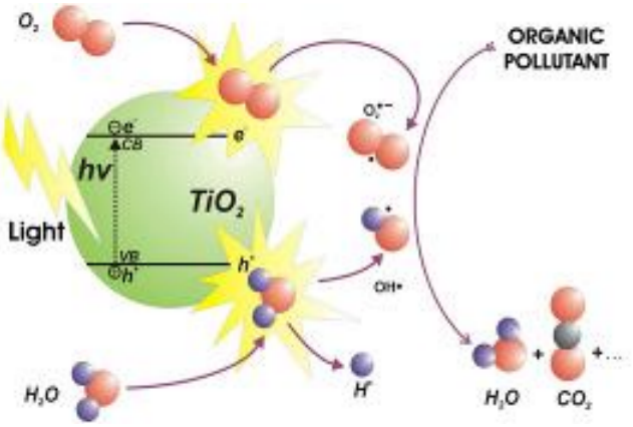

Figure 1.2: Photocatalytic effect on TiO_2 nanoparticles [13].

- fuel cell

  TiO_2 nanoparticles have been considered as a support for electrocatalysts of fuel oxidation. After doping Ti-NT with palladium or gold atoms it shows better catalyst properties than traditional Pd/C or Au/C catalyst. The enhancement of catalyst performance is due to the structural water and increased resistance to poison by CO (Bavykin and Walsh [12]). Ti-NT with Au have better catalyst property then a conventional Au/Al_2O_3 [14].

- lithium batteries

  Nanoparticles are widely used in rechargeable lithium batteries. The potential of utilizing Ti-NT are due to their mesoporous structure and effective transport of lithium ions. In lithium batteries there are three steps of charging/discharging of batteries: diffusion of lithium ions in the electrolyte, diffusion of intercalated ion and the electrochemical reaction. By using the Ti-NT, the rate of diffusion of intercalated lithium ions has been improved. The small size of lithium ions allows an interlayer transport of Li^+ within the Ti-NT tubular structure (Bavykin and Walsh [12]) (Figure 1.3).

- solar cells

  Ti-NT have been studied for applications as electrodes for dye-sensitized solar cells. The main advantage of using Ti-TN is their elongated structure that is utilized in the transport of electrons to the electrode. Powder materials, which have poor transport properties due to random orientations of crystallites, were studied as well.

  Fortunately, it is possible to prepare Ti-NT directly on the electrode (Bavykin and Walsh [12]). The principle of transport of electrons is shown in Figure 1.3.

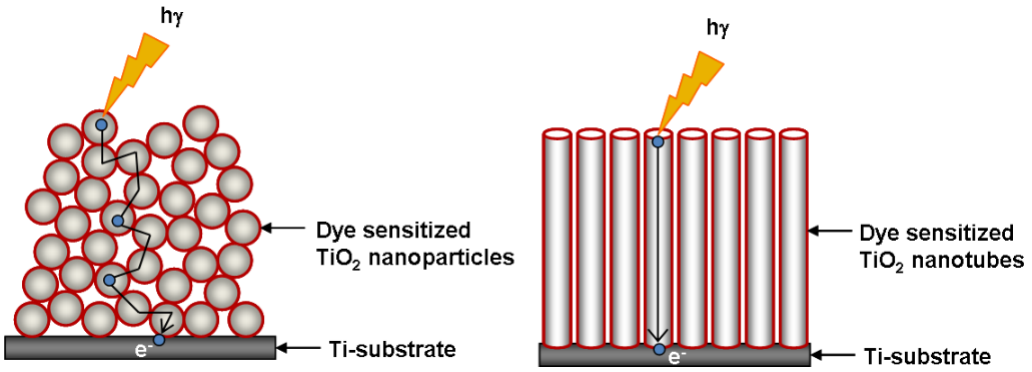

Figure 1.3: Transport of electrons in dye-sensitized solar cell [13].

- hydrogen storage

  Two different mechanisms are used for hydrogen storage materials: physisorption and chemisorption. The former is characterized by weak interaction between material and hydrogen but it is necessary to use low temperatures and high pressures to take up hydrogen. The latter with stronger interaction between material and hydrogen needs high temperatures for the release of the hydrogen gas from the material.

There is a need to find some other materials with interaction between these two techniques, having strong interaction but at low temperatures. Luckily, the Ti-NT shows a wide temperature range of uptaking the hydrogen gas (-196°C to 125°C) (Bavykin and Walsh [12]).

- biomedical application
  Inorganic nanocrystalline materials were used for controlling drug delivery and labelling of biological samples. Ti-NT layer on Ti bulk material can be used in orthopedic or dental applications because the cells are easier to stick to surfaces covered by Ti-NT than to pure metal. This is the reason why it may be used in implants (Bavykin and Walsh [12]). Balasundaram et al. [15] observed that new bone cells can grow easier on Ti surface covered by nanotubes. After doping Ti-NT by calcium a good bone regeneration was obtained in a living body (implantation in rat) (Kasuga [16]). The biocompatibility of Ti-NT was studied by Lopez et al. [17] - Ti-NT was stable and did not make any major changes of rat's brain in period of six months.

- composite
  The mechanical, thermal and electrical properties of polymer-based composites could be improved after addition of nanotubes [18]. The addition of Ti-NT to polymers matrix increase Young's modulus of the composites. Similar studies were done by Kralova et al. [19] and they showed that the increase of the elastic modulus of composites after addition of Ti-NT are 35% but addition of nanocrystalline powder of TiO_2 increase the elastic modulus of composite only by 14%.

- magnetic material A nanosized semiconductor with magnetic properties is interesting for spin based devices. Ti-NT are naturally paramagnetic. In order to obtain magnetic moment they have to be doped by magnetic ions. Ferromagnetic as well antiferromagnetic properties have been observed after doping Ti-NT by ions of Co^{2+}. The final magnetic state depends on Ti:Co ratio. For deposited nickel nanoparticles on the surface of Ti-NT ferromagnetic properties has been found. On the other hand theoretical studies of doping by Fe^{3+} show magnetic insulator (Bavykin and Walsh [12]).

1.3. Structure of titania (titanate) nanotube

The structure of Ti-NT has not still be well understood. It was found, that the structure depends on preparation conditions - for the hydrothermal synthesis the temperature is probably the most significant factor. The common property of Ti-NT often published in the literature is the multiwall structure of the nanotube and outer diameter of the nanotube between 7 - 10 nm [20], [21]. Sodium ions could be present within the structure as a residue from the hydrothermal syntesis, see below.

Big effort has been devoted to studies of possible structure of titania/titanates nanotubes. The situation is quite complicated because different methods are used for Ti-NT preparation. Recently, in particular hydrothermal reaction has been widely used. In the following paragraphs, we summarize many published structures of Ti-NT.

Seo et al. [22] discussed the preparation temperature of structure of Ti-NT. For low temperatures, they obtained **amorphous phase** which was crystallized in anatase form at higher temperatures and this transformed to rutile with further heating. At higher preparation temperatures, **the anatase structure** appeared immediately. The anatase structure of Ti-NT was the first suggested structure of Ti-NT by Kasuga et al. [2]. They also obtained Ti-NT with outer diameter of about 8 nm [23]. This structure was also reported by other authors, for example by Peng et al. [24], Wu et al. [25]. They observed Ti-NT with diameters in the range of 8-12 nm. Zhang et al. [26] reported anatase with multiwall structure of nanotubes - the thickness of the multiwall Ti-NT was found in the range of 2 - 5 layers. Wang et al. [27] supposed that Ti-NT have anatase structure with outer diameter approximately 9 nm and the nanotube was created by rolling two-dimensional (2D) sheet. The nanotube had spiral base and open ends. Similar results with spiral shape and diameter around 10 nm were reported Yao et al. [28]. Wang et al. [29] supposed that the structure of Ti-NT should be **nonstoichiometric TiO_2**. However, their powder X-ray diffraction pattern showed a mixture of anatase and rutile phase. Another possible structure could be **hydrated phase $TiO_2 \cdot H_2O$** or a titanate as found by Lan et al. [30]. These authors also described the morphology - tubes or rods - depending on the preparation temperature. The structure of Ti-NT depends on it as well.

Brookite structure of Ti-NT was found by Deng et al. [31]. Obtaining of this structure of Ti-NT is more complicated. This is a two-step procedure: preparation of 'normal' Ti-NT (normal preparation condition as other mentioned Ti-NT) and transformation to brookite.

β **phase of TiO_2** was identified as a structure of Ti-TN as well [32].

Armstrong et al. obtained a multiwall structure of Ti-NT with the outer diameter of the nanotube between 10 and 20 nm. This structure of Ti-NT was also obtained by Sutrisno [33]. He observed a multiwall structure with 1-3 layers and outer diameter in the range of 5-8 nm.

Another possible structure of Ti-NT is $\mathbf{H_2Ti_3O_7}$ (Predham et al. [34]) or its **sodium salt** $\mathbf{Na_2Ti_3O_7}$ (Kim et al. [35]). This structure was reported by Zhu et al. [36] - multiwall Ti-NT (3-4 layers) with outer diameter of about 10 nm. The authors supposed that their Ti-NT contained some sodium ions. The same outer diameter of Ti-NT was obtained by Yoshida et al. [37]. Minority of sodium ions was observed in their Ti-NT. Ti-NT can also have the structure of $H_2Ti_3O_7$ or $Na_2Ti_2O_4(OH)_2$ [38]. The authors assume the structure of $H_2Ti_3O_7$ as more probable. They discussed possible formation of the shape of Ti-NT. It could be spiral, concentric circle or onion-like shape. They obtained open ends multiwall (typically four walls) Ti-NT with constant diameter along the nanotube. Du et al. [39] reported multiwall nanotubes with spiral base and diameter of about 9 nm. Surprisingly, Kasuga [16] reported this structure of Ti-NT with outer diameter of about 8 nm. Yuan and Su [40] discussed the influence of temperature of hydrothermal treatment on the structure of Ti-NT and their transformation to nanofibers and nanowires. They obtained multiwall (1-5) Ti-NT with diameters in the range of 8 - 10 nm. Raman spectroscopy and EXAFS study of this structure, ($H_2Ti_3O_7$), is described in [41] by Ma et al.

These authors also reported the structure of **lepidocroite titanate** ($\mathbf{H_xTi_{2-x/4}\square_{x/4}O_4}$ ($\square$ represent vacancy)) in their earlier article [42]. They obtained nanotubes with outer diameter of approximately 10 nm and they proposed this structure rather than trititanate ($H_2Ti_3O_7$) owing to thermogravimetry studies - lepidocroite titanate loose weight more quickly than trititanate.

Another possible structure of Ti-NT have been reported - $\mathbf{H_2Ti_3O_7{\cdot}nH_2O}$ or $\mathbf{Na_xH_{2-x}Ti_3O_7{\cdot}nH_2O}$ ($0 < \mathrm{x} < 2$) [43]. Morgado et. al [44] got Ti-NT with 3 - 5 layers and with outer diameter in range from 7 to 10 nm. Their structure is $Na_xH_{2-x}Ti_3O_7{\cdot}nH_2O$ ($0 < x < 2$) and n should be less than 1.2. In their latter article [45] they described changes of diameter of the nanotube by changing the crystal size of initial TiO_2 powder (220 and 8 nm). The structure $H_2Ti_3O_7{\cdot}nH_2O$ with $n \sim 0.8$ was obtained by Thorne et al. [46]. They found multiwall nanotube too.

It is also possible to find a structure of Ti-NT $\mathbf{Na_xH_{2-x}Ti_2O_4(OH)_2}$ [47] ($0 < x < 2$). Kubota et al. [47] supposed that the structure should be lepidocroite titanate. Ti-NT with four walls outer diameter approximately 9.3 nm and with the structure of $Na_xH_{2-x}Ti_2O_4(OH)_2$ was obtained by Yang et al. [48]. They reported that x depends on pH used at the post-preparation

of the final solution from synthesis. After the synthesis the solution is neutralized by HCl as it will be mentioned in chapter 4. This layer structure was obtained by Zhang et al. [49] either.

The structure of $\mathbf{H_2Ti_2O_5{\cdot}H_2O}$ [50] was reported by Tsai et al. [50]. By changing of the pH value it was possible to interchange sodium ions to hydrogen in the structure. The morphology of Ti-NT of the same structure was studied [51] as a function of pH. For very low pH value only nanoparticles and no nanotubes were found. Chen et al. [52] gained the structure of Ti-NT as $Na_2Ti_2O_5{\cdot}H_2O$ where sodium ions could be replaced by hydrogen by acid washing. They also studied the necessary time to obtain Ti-NT and their process of formation. They obtained multiwall nanotubes. Xu et al. [53] used $H_2Ti_2O_5{\cdot}H_2O$ Ti-NT to prepare rutile or anatase nanoparticles with different size. Ti-NT were washed by acid to lower the pH value. Kochkar et al. [54] got this structure of Ti-NT with outer diameter approximately 10 nm. Yan et al. [55] obtained the same outer diameter as Kochkar et al. [54] , but Yan et al [55] had smaller inner diameter.

Nakahira et al. [56] suggested structure of Ti-NT as of the compound $\mathbf{H_2Ti_4O_9{\cdot}H_2O}$. This structure was obtained for different synthesis temperature. From their TEM studies, the nanotube had multiple shells and diameter smaller than 10 nm.

To conclude this chapter, different reported structures of Ti-NT are summarized:

- ⇝ anatase structure of TiO_2 - tetragonal lattice system with space group I 4_1/a m d [57]
- ⇝ brookite structure of TiO_2 - ortorombic lattice system with space group P b c [58]
- ⇝ β-TiO_2 - monoclinic lattice system with space group C 2 /m [59]
- ⇝ $H_2Ti_3O_7$ ($Na_2Ti_3O_7$) - monoclinic lattice system with space group C 2 /m [60]
- ⇝ $H_2Ti_3O_7 \cdot nH_2O$
- ⇝ $H_xTi_{2-x/4}\square_{x/4}O_4$
- ⇝ $H_2Ti_2O_5 \cdot H_2O$ ($Na_2Ti_2O_5 \cdot H_2O$) - orthorombic lattice system with space group P [61]
- ⇝ $H_2Ti_2O_4(OH)_2$ ($Na_2Ti_2O_4(OH)_2$ - orthorombic lattice system with space group I [62])
- ⇝ $H_2Ti_4O_9 \cdot H_2O$ - monoclinic lattice system [63]

Almost in all articles about Ti-NT were mentioned that Ti-NT have multiwall structure with 2 to 5 layers. Outer diameter is in range from 7 nm to 12 nm.

2. Aim of thesis

Different remarkable properties of Ti-NT have been introduced in previous chapters. However, as it has been emphasized, quite many different structural models of Ti-NT were proposed.

The main aim the present work was to identify the structure of Ti-NT prepared via hydrothermal synthesis from different initial TiO_2 powders. Mainly X-ray diffraction (XRD) and electron microscopy (EM) were applied. The work was performed in the following steps:

- Identification of the structure of Ti-NT
- Building the structural model of Ti-NT
- Calculation of X-ray powder diffraction patterns by using the models and comparison with the experimental data

3. Theory

Study of the crystal structure of Ti-NT was done mainly by XRD and transmission electron microscopy (TEM). Other methods like energy dispersive spectroscopy (EDX) and scanning electron spectroscopy (SEM) were performed to obtain more information about the samples.

3.1. Electron crystallography compared with X-ray crystallography

The X-ray crystallography is still the best technique for determination of the crystal structure. About 90 % of new structures are detemined by X-ray diffraction. However, the electron crystallography has some advantages and can be well complementary to the X-ray crystallography:

- ☻ high resolution transmission electron microscopy (HRTEM) images can be used for study of lattice defects in crystals
- ☻ electrons interact much stronger with the matter than X-rays - for TEM smaller samples can be sufficient than for XRD
- ☻ different interaction between electrons - crystal and X-rays - crystal, X-rays detect electron density distribution in crystals, while electrons detect electrostatic potential distribution in crystals
- ☻ electron can be focused by electrostatic or electromagnetic lens to obtain image, the phase information can also be obtained

The combination of XRD and electron diffraction (EM) can be very helpful [64].

3.2. X-ray diffraction

Basic equation of X-ray diffraction is the well-known Bragg equation relating the position of the diffraction maximum and the interplanar spacing d of the corresponding diffraction planes (hkl):

$$2\,d_{hkl}\,sin(\theta) = n\,\lambda \tag{3.1}$$

where λ is the wavelength of the used X-ray radiation and θ is the scattering angle. The analysis of the geometry of the diffraction pattern usually

allows the determination of the symmetry and geometry of the lattice cell. However, in order to determine also the positions of individual atoms, i.e. the crystal structure, the analysis of intensities of many diffraction lines is necessary.

X-ray photons are scattered mainly by electrons, so the intensities of diffraction lines are related to the electron density. The measured intensity is proportional to the square of the structure factor:

$$I_{hkl} \approx |F_{hkl}|^2$$

where the structure factor of the crystal is related to the scattering by the unit cell and contains the information on the atomic positions in the unit cell. It is described by following formula (3.2):

$$F_{hkl} = \sum_{i=1}^{N} f_i \, e^{2\pi i \, (hx_i + ky_i + lz_i)} \tag{3.2}$$

where x_i, y_i, z_i are fractional coordinates which represent relative position of atom i in the unit cell, and f_i is the atomic scattering factor which could be described as the Fourier transformation of electron density ρ:

$$f = \int_V \rho(\vec{r}\,) \, e^{i\vec{Q}\cdot\vec{r}} d^3r \tag{3.3}$$

The atomic scattering factors can well be calcualted with the aid of formula:

$$f(\theta, \lambda) = \sum_{i=1}^{4} a_i e^{-b_i \left(\frac{\sin\theta}{\lambda}\right)^2} + c \tag{3.4}$$

where the coefficients a_i, b_i, c are tabulated for all atoms (sometimes also in ionized state) in the International Tables for Crystallography. The structure factors can also be calculated easily by different available crystallographic software. For example for structure databases, crystal structure visualization or structure refinement.

In general, the structure factor is complex, thus it could be described by its phase φ and apmlitude [65] [66]:

$$F = |F| \, e^{i\varphi}$$

3.2.1. Phase problem of X-ray diffraction

Since in the diffraction experiment only the intensities of reflections are measured, the information on the phases in structure factors are lost. For centrosymmetric crystals the phases are equal to 0 or π but for noncentrosymmetric cryslals could phase be in range of $(0, \pi)$. There are several methods used for solution of this phase problem. The short list of some methods is below, more information could be found in [66]:

- heavy-atom method If our sample contains only a few heavy atoms, the structure factor can be split into two parts - the first depends only on heavy atoms and the second depends on the rest of atoms. The first step is to find positions of heavy atoms and the light ones could be obtained by iterative procedure based on Fourier transformation of electron density. Positions of heavy atoms can be obtained from the Patterson function - autocorrelation function of electron density which can be constructed from the measured integrated intensities I_{hkl}. The strong maxima of the function correspond to the distances between heavy atoms. Moreover, the function show the same symmetry as the crystal structure.

- isomorphous replacement In this method, some light atoms or light organic compound are replaced by heavy atoms. Positions of these atoms are then located. It is assumed that the structures are isomorphous.

- anomalous scattering At least two different wavelengths are used. One wavelength is near the absorption edge of heavy element in the structure which results in signicant change of the structure factor due to the change of the corresponding atomic factor of the element. However, this type of experiment has to be preformed only synchrotron radiation (tunable λ).

- direct methods Direct methods of determination of phases are based on different statistical relations applied on structure factors and on the search of suitable groups of reflections - structural invariants.

3.2.2. Powder X-ray diffraction

Crystal structures should be preferrably solved from the single crystal diffraction. However, in many cases this is not possible because suitable single crystals are not available. It is often no easy to prepare them. Therefore, methods of structure determination or structure refinement from powder

diffraction have been elaborated and they are quite widely used nowadays, even if there is less information in powder diffraction pattern (actually, this is one-dimensional (1D) projection of three-dimensional (3D) picture from single crystal)

In general, powder diffraction can give information on several structural and microstructural features as well as on the composition of the studied samples:

- phase identification
- lattice parameters
- crystal structure
- residual stress
- prefered orientation - texture
- line profile analysis - crystallites size, microstrain, dislocation density

The information can be obtained either be the analysis of individual diffraction lines or by the Rietveld refinement. This method is based on the description of full PXRD pattern by analytical (in most cases) functions representing all necessary effects: crystal structure, microstructure (crystallite size, microstrain), preferred orientation, instrumental aberrations, background etc. Corresponding parameters of the functions come out from a mathematical model and they are found by a least-squares minimalization of the weighted difference between obseved and calculated intensities [65].

3.2.3. Amorphous and not well crystalline materials

All the above methods are well elaborated and often used for well crystalline samples. However, they cannot be used for disordered compounds like gases, liquids, amorphous solids, nanocrystalline powders with very small particles (below about 4 nm) or different kind of nanostructures like nanotubes, nanorods. In these cases, usually all atoms in the particles or diffracted volume must be taken into account. It is not possible or sufficient just to describe the unit cell. Then the Debye scattering equation can be applied [67]:

$$I_{eu} = \sum_m \sum_n f_m f_n \frac{\sin qr_{mn}}{qr_{mn}} \tag{3.5}$$

where eu means electron units, f_m is the atomic factor of the atom m and q is the diffraction vector magnitude. The Debye formula describes the

intensity distribution spherically averaged over the reciprocal space. The sum runs over all the pair distances r_{nm} of the atoms n, m. The formula is valid for any form of matter and there is no limitation on the number of different kinds of atoms in the sample. This can put large demands on the computing time in case of larger particles. Anyway, this old formula has become more popular recently for modelling of X-ray scattering from nanoparticles.

3.3. Transmission electron microscopy

Electrons are negatively charged particles and they strongly interact with atoms via Coulombic forces. This strong interaction leads to one disadvantage - the samples for TEM must be very thin. It is also very important to work with a good vacuum to avoid scattering by gas molecules.

Electrons are quantum particles - we can observe both the particle and wave properties. Since electrons are charged they can be focused by electromagnetic or an electrostatic lenses. Therefore, the electron microscopes can be well constructed. There are two types of electron microscopes - transmission and scanning electron microscopes.

If an aperture is inserted into back focal plane of objective lens in TEM and direct beam is selected, a bright-field image is created by elastically scattered electrons. If diffracted beam is selected, dark-field image is obtained. In HRTEM, an image is created due to phase difference of scattered electromagnetic waves and in principle it is possible to display atomic structure of a specimen.

3.3.1. Phase contrast, contrast transfer function and high resolution electron microscopy

The phase object approximation - the electrons passing through the crystal samples have only phase shift - electrons can be only elastically scattered and scattered electrons are almost parallel to the incident beam due to high energy of the electrons. For thick samples there may be two other effects - a multiple scattering and a non-linear effects which depend on the interference of different waves. If a crystal is so thin that these two effects could be ignored, the crystal is considered as a weak phase object. The phase shift of the electrons depends on the accelerated voltage and the projected potential of the crystal.

3.3.1.1. Contrast transfer function

Scattered waves carry information on the projected potential in the form of phase shift. When the crystal is thin and the lenses are in focus, there is only small contrast in the image. An extra phase shift can be introduced by the aberrations of the lenses, which modulates the amplitude of the scattered beam in real space. Its effects can be described by the so-called contrast transfer function (CTF). This function has two parts - an oscillation part, which determines the contrast of the image, and an envelope part, which determines the resolution of the image and depends on the amplitude of spatial frequency component. If the image is taken from a weak phase object at Scherzer defocus (at this defocus the point resolution is achieved and it can be calculated from spherical aberration of microscope and accelerating voltage), it directly represents the projected potential of the crystal. In images only the intensity (square of the amplitude of wave function) is recorded and the phase part of the wave function is lost. However, the phases of structure factors of the crystal are present in the image and can be recovered using crystallographic image processing [64].

3.3.1.2. Solving crystal structures from HRTEM images by crystallographic image processing

If the HRTEM images is affected by the following factors, it will be very difficult to interpret the images directly in terms of the structure.

- Random noise
- Electron optical distortions of the microscope; beam tilt, defocus, astigmatisms
- Crystal tilt

In order to utilize crystallographic image processing to study crystal structures, it is important to:

- Use the thinnest part of the crystal to avoid multiple scattering and non-linear effects, and an amorphous area to find CTF.
- Record a set of HRTEM images with different defocus value to facilitate CTF determination and avoid CTF crossover problems.
- Determine the 3D structure - combine images taken along different zone axis

☻ Use a magnification such that the finest details in the sample can be seen.

If radiation damage is not a problem, longer exposure time should be used to increase the signal-to-noise ratio.

3.3.1.3. Through-focus series method

The information contributed by the kinematical scattering can be maximized and the double scattering can be minimized by combining a series of through-focus images. Therefore structures can be determinate more accurately and reliably [64]. This method uses through-focus series of HRTEM images and defocus values and 2-fold astigmatism of the images can be automatically determined and compensated for.

3.4. Scanning electron microscopy

In scanning electron microscope the electron beam is scanning selected area of the specimen. Thus the information on topography of the surface and the chemical composition of the sample can be obtained. Focused high energy electron beam interacts with the sample and secondary electrons, characteristic X-ray radiation, back scattered electrons are produced. Back scattered electrons are the electrons which are elastically scattered from the surface of the sample. Their intensity strongly depends on atomic number of the elements contained in the specimen. Therefore, they are used for mapping of the distribution of different chemical elements in the sample. Secondary electrons are produced by the interaction of the primary beam with the specimen (inelastic stattering) and carry information about the surface topography([68]).

3.5. X-ray energy dispersive spectroscopy

EDX is an analytical method used for determination of compounds of a sample. Principle of the method is the following. The beam excites an electron in an inner shell of an atom, ejecting it from the atom. An electron from an outer shell falls to the inner shell, filling the whole and emitting an X-ray photon with the energy equal to the difference between the energies of the two shells. Energy of photon is characteristic for each element in the periodic table. The principle of EDX is shown in the Figure 3.1.

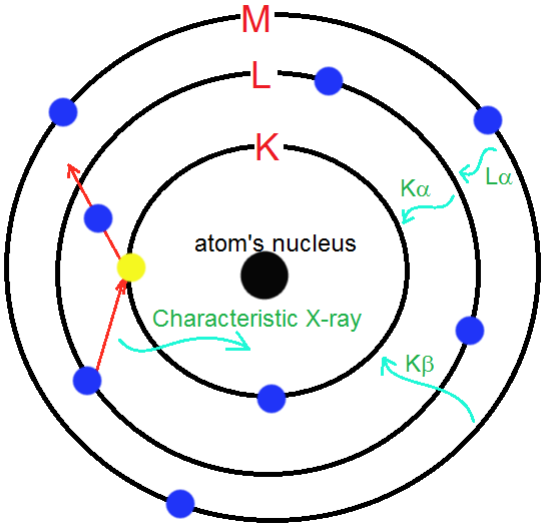

Figure 3.1: Principle of EDX (characteristic X-rays are emitted by electron beam irradiation of the sample).

4. Preparation of Ti-NT

Synthesis of Ti-NT is based on the hydrothermal treatment of TiO_2 powder.

4.1. Phases of TiO_2

TiO_2 has two most common known phases with different crystal structure - anatase and rutile. Both are commercially available. Rutile is the most stable phase and the other phases usually transform to it during the heating. The crystal structure of **rutile** is tetragonal with the space group P 4_2/ m n m and lattice parameters [69]:

$$a = 4.593\,\text{Å},\ b = 4.593\,\text{Å},\ c = 2.959\,\text{Å}$$

The crystal structure of the rutile is shown in Appendix 1 in different orientations and one specific orientation is in Figure 4.1b. The projection was done by program J-Mol [70].

Anatase has also tetragonal crystal structure but with the space group I 4_1/a m d and lattice parameters [57]:

$$a = 3.785\,\text{Å},\ b = 3.785\,\text{Å},\ c = 9.514\,\text{Å}$$

Projections of the unit cell are in Appendix 2 and one specific orientation in Figure 4.1a.

Both phases of TiO_2 were used in synthesis of Ti-NT. Another common phase of TiO_2 is **brookite**. It has orthorombic crystal structure, space group P b c a with lattice parameters [58]:

$$a = 5.456\,\text{Å},\ b = 9.182\,\text{Å},\ c = 5.143\,\text{Å}$$

Different orientations of the brookite stucture are shown in Appendix 3 and one specific orientation in Figure 4.1c.

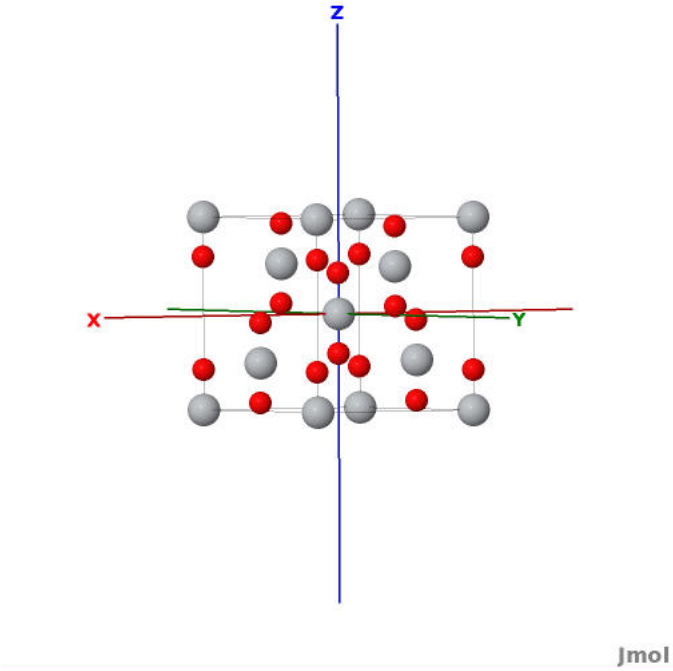

(a) Model of anatase

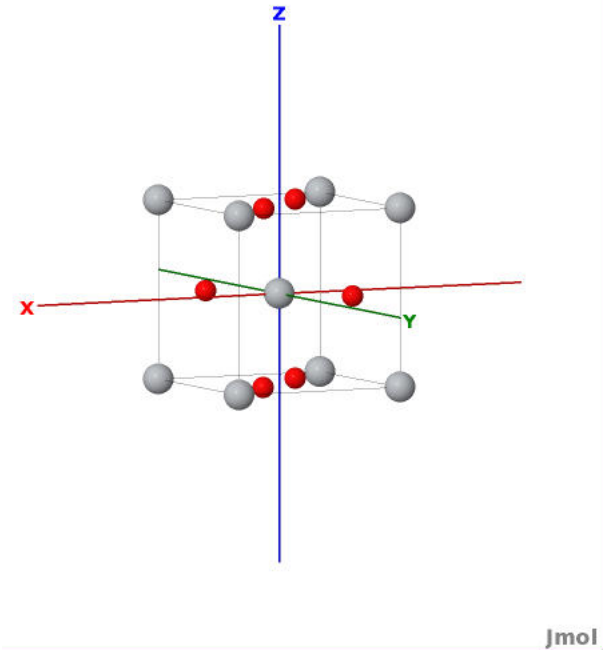

(b) Model of rutile

Figure 4.1: Schematic pictures of crystal structures of three TiO_2 phases in general orientation. See Appendix 1-3 for more.

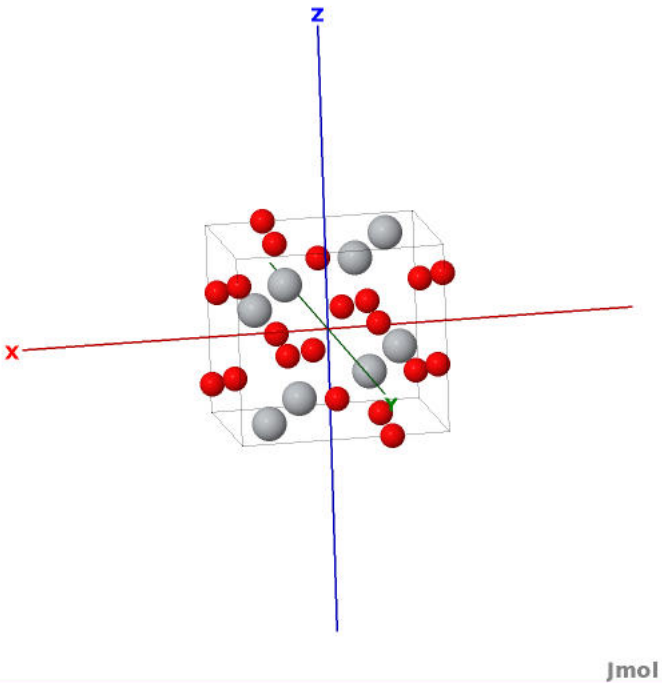

(c) Model of brookite

Figure 4.1: Schematic pictures of crystal structures of three TiO_2 phases in general orientation. See Appendix 1-3 for more.

4.2. Preparation of samples

Commercially available anatase nad rutile powders with two different particle size - in nano and micro range were utilized. Brookite nanopowder was synthetized in Institute of Inorganic Chemistry, Academy of Science of the Czech Republic, v.v.i. The grain size of powders are displayed in Table 4.1.

Table 4.1: The grain size of different TiO_2 powders and their notation in the text

phase of TiO_2	size
microrutile	1 μm
nanorutile	50 nm
microanatase	1 μm
nanoanatase	38 nm
brookite	100 nm

Ti-NT were prepared from these powders in Institute of Macromolecular Chemistry, Academy of Science of the Czech Republic, v.v.i. The preparation procedure concists in a hydrothermal treatment of the initial TiO_2 powder. The reaction could be written as:

$$TiO_2\ powder + NaOH \xrightarrow{heat} Titanate\ nanotubes$$

The process of synthesis could be described by following way: the initial TiO_2 powder is put in 10M NaOH aqueous solution into a closed vessel and was heated at 120°C for 48 hours. After that the product was washed with a water and neutralized by 0.1M HCl aqueous solution to obtain pH 5.5. Then the product was filtered in membrane filtered device with gas nitrogen and water. The final product was obtained by a lyophilization. The lyophilization is a method for removal of residual water from Ti-NT in order to get a dry product of Ti-NT. The final dried Ti-NT had tubular shape. The tubular shape was created during the hydrothermal synthesis. Chemical composition was determined by EDX in [71]. No residual sodium ions were found. More details about synthesis and SEM images of Ti-NT could be found in [71] and [72].

5. Experimental setup

Samples of Ti-NT were analyzed by XRD and TEM. TEM investigation were performed at the Institute of macromolecular chemistry, Academy of Science, v.v.i. and at the Stockholm University, Department of Materials and Environmental Chemistry. For characterization by XRD two diffractometers were used - in transmission and reflection geometry, respectively. Samples of Ti-NT look like a feathers, photo of the sample is shown in Fig.5.1.

Figure 5.1: Picture of Ti-NT look like a feathers, glass capillary has diameter approximately 0.5 mm.

5.1. Sample preparation for X-ray measurement

For X-ray measurement, two different diffractometers were utilized. The sample preparation for X-ray measurement required one common task - to prepare powder from 'feather' samples.

- for transmission geometry: For placing enough sample directly to the beam a copper-wire holder had been used. This holder is shown in Figure 5.2. To obtain enough sample in the copper-wire holder, a mash of Ti-NT with ethanol was prepared and placed into the cooper-wire holder.

Figure 5.2: Picture of Ti-NT in cooper-wire holder, diameter of wire is 0.65 mm.

- for reflection geometry: The sample of Ti-NT was put on a glass holder and mixed with ethanol as in previous case. Then the mash was put on the glass holder and relatively flat surface was prepared. The specimen had to be dried at the room temperature before the measurement. Otherwise, additional background (very wide maximum) was observed.

5.2. X-ray diffractometer

- X-ray diffraction in transmission geometry: For this type of geometry X-ray diffractometer Rigaku Rapid II have been used.

  Rigaku Rapid II diffractometer was equipped with large 2D image plate detector and Mo-Kα X-ray tube. In primary beam a graphite Kα_{12} monochromator was placed followed by the collimator of 0.3 mm diameter. The instrument with the Ti-NT specimen in the cooper-wire holder is shown in Figure 5.3.

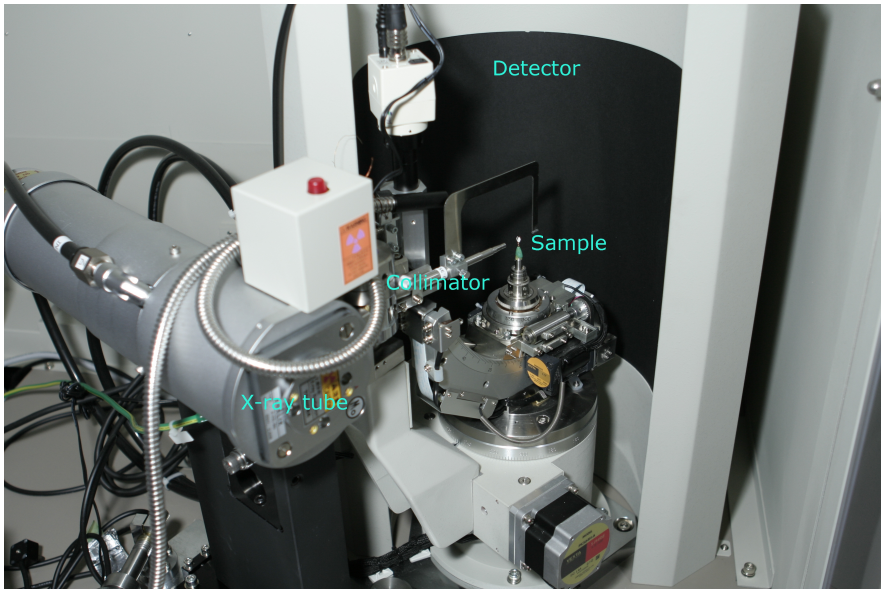

Figure 5.3: Picture of Ti-NT in cooper-wire holder in Rigaku Rapid II diffractometer.

Typical 2D measured diffraction data is in Figure 5.4. The exposure time was about 30 min. in the used geometry. This 2D data was converted by the software 2DP into a conventional powder X-ray diffraction (PXRD) pattern. This pattern is shown in Figure 5.5.

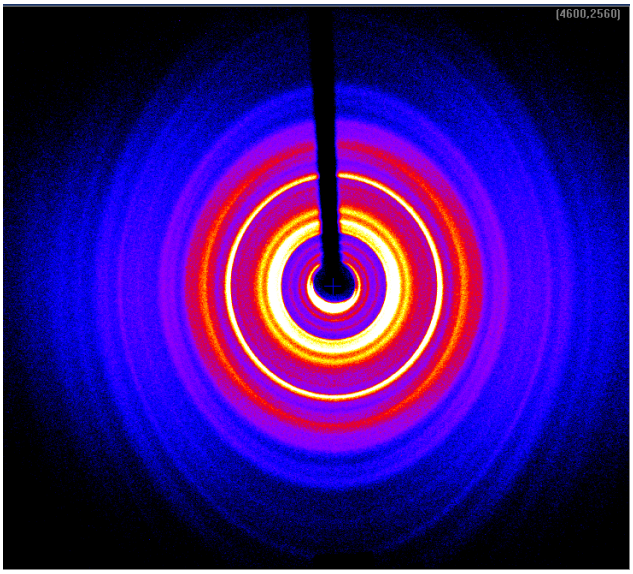

Figure 5.4: 2D diffraction data from Ti-NT.

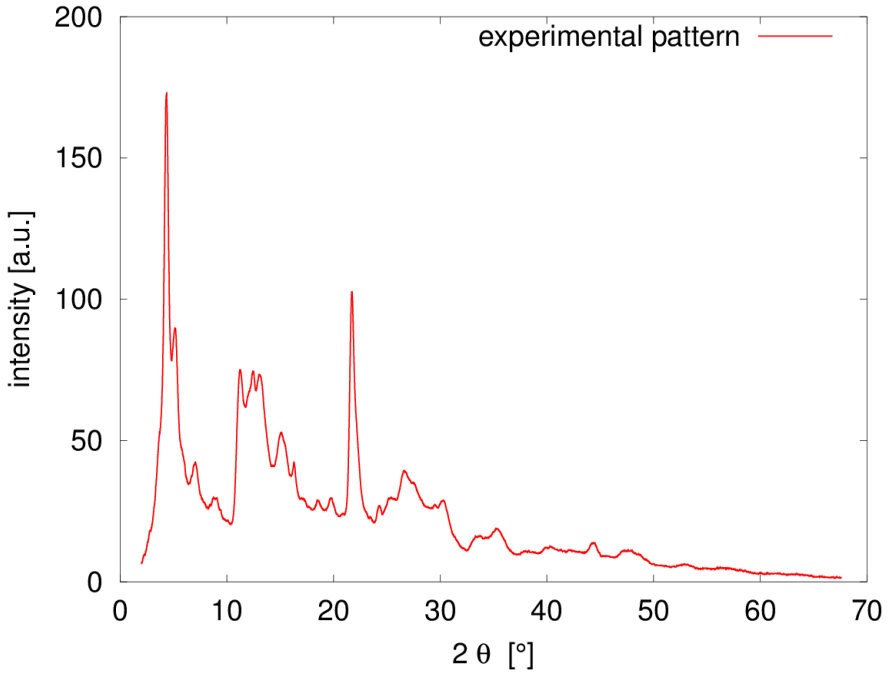

Figure 5.5: PXRD data of Ti-NT (prepared from rutile) converted from measured 2D data.

- X-ray diffraction in reflection geometry:

  - Bragg-Brentano geometry (BB) For this type of geometry PANanalytical MPD diffractometer was used. The experimental setup is shown in Figure 5.6. Measurement was performed by conventional BB symmetric $\theta - 2\theta$ scan.

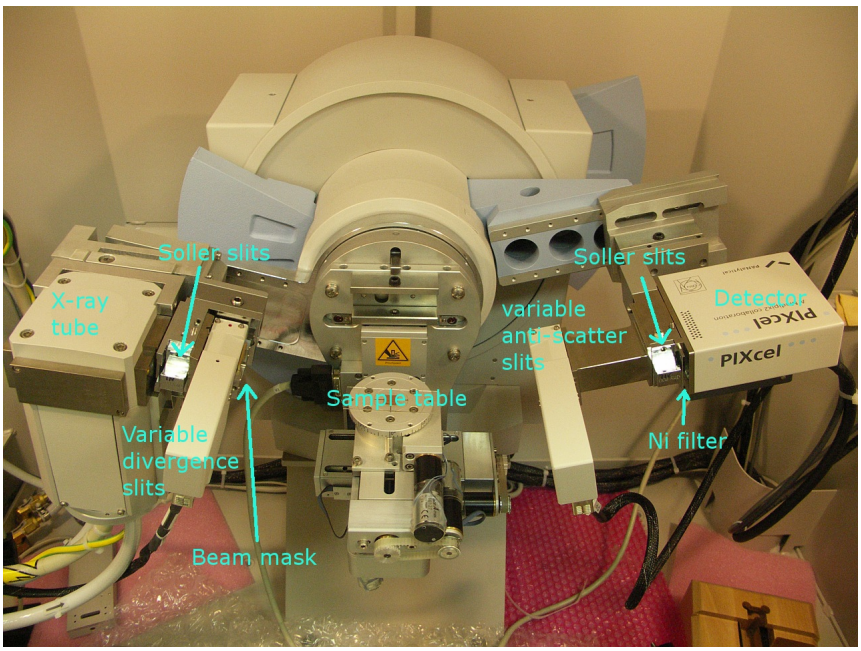

Figure 5.6: Picture of MPD diffractometer.

0.04 rad Soller slits, 5mm beam mask and variable divergence slits were placed in the primary beam and variable anti-scatter slits together with nickel filter for elimination of Cu-Kβ radiation were used in the diffracted beam.

- For estimation of texture influence, PANanalytical MRD diffractometer was used. This diffractometer is equipped with the Eulerian cradle. X-ray tube with point focus, polycapillary optics and point detector were utilized in this type of experiment.

  Cu-Kα radiation was used in all the experiments in reflection geometry.

5.3. Sample preparation for electron microscopy

The sample preparation for HRTEM and TEM was the same. A small amount of a sample was ultrasonically dispersed in ethanol. A drop of suspension was put on holey carbon coated copper grid. Then the prepared sample was dried.

The sample preparation for SEM and EDX studies was the following: in the first step powder sample was prepared. The suspension of sample with ethanol was dried and then put on a carbon gluing tape. This tape was directly placed in the microscope.

5.4. Electron microscopes

Three different microscopes was utilized:

- HRTEM image was taken by JEOL JEM 2100F TEM. 200keV accelerated voltage and field emission gun (FEG) was used. This studies (HRTEM) was done at Stockholm university during ERASMUS studies.
- TEM was performed on 120 kV Tecnai G^2 Spirit 120 with LaB_6 emission gun. TEM investigation was done at the Institute of Macromolecular Chemistry, Academy of Sciences of the Czech Republic,v.v.i.
- For SEM and EDX studies Tescan Mira microscope was used. This microscope has autoemission electron gun which operated at 15 keV. This investigation was done at Faculty of Mathematic and Physics, Charles University in Prague.

6. Computer simulations and phase identification of Ti-NT

Three different structural models were constructed and used for the calculations of powder X-ray diffraction patterns by using the Debye formula (3.5, [73]). The models were based on the literature data as well as our own observations.

Enyashin and Seifert [74] studied Ti-NT with anatase structure. They used two models of Ti-NT - zig-zag nanotube and armchair nanotube (their definitions is given in following subchapter) for studies of the thermal stability of nanotubes and their electronic properties. Ma et al. [75] observed that Ti-NT are developed from 2D sheet. 2D sheets became unstable in NaOH solution and tubular structure grew up. Tubes had multiwall structure with 3-6 layers. Zhang et al. [76] obtained Ti-NT with structure of $H_2Ti_3O_7$ and studied it by the first principle ab-initio calculations based on the density functional theory. They suggested that Ti-NT were developed from corresponding structure plate.

6.1. Anatase nanotube

As mentioned above, anatase is one of the well-known phases of TiO_2 and one of the published structures of Ti-NT (see chapter 1). The anatase structure was considered because our samples of Ti-NT should not contain any sodium ions, as it was found by chemical analysis in [71].

In some orientations of the anatase structure hexagon-like polygons made of titanium atoms can be found [77]. This layer of the anatase structure is the [101] surface and it is shown in Figure 6.1.

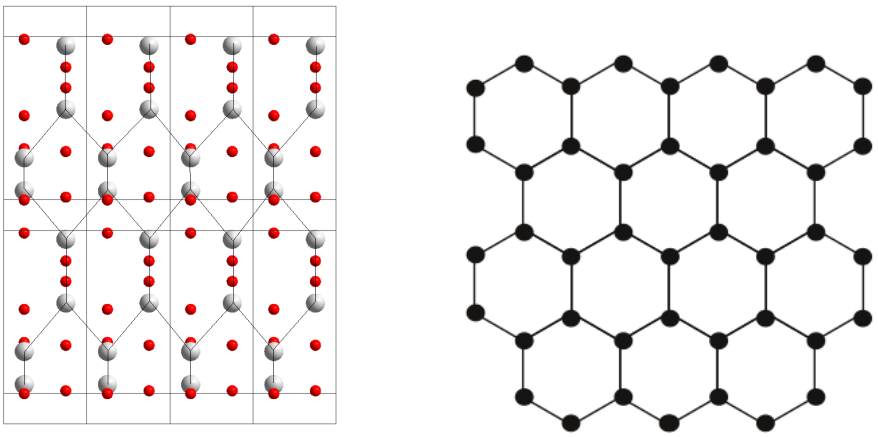

(a) anatase 101 plane (b) hexagons from carbon atoms

Figure 6.1: Layer [101] of anatase displaying hexagons like structure (a) and hexagons in graphene (b).

Thus the anatase nanotube could be described by chirals vector in honey comb lattice as in the carbon nanotube. The chiral vector (C_h) in the carbon nanotube [78] is defined by two vectors a_1 and a_2 in the hexagonal lattice by following formula (6.1):

$$C_h = na_1 + ma_2 \tag{6.1}$$

where the m and n are integers which have to fulfil the following condition:

$$0 \leq |m| \leq n$$

The definition of vectors a_1 and a_2 in the hexagonal lattice is shown in Figure 6.2.

The chiral vector could be also rewritten in shorter way using numbers m and n:

$$C_h = (n, m)$$

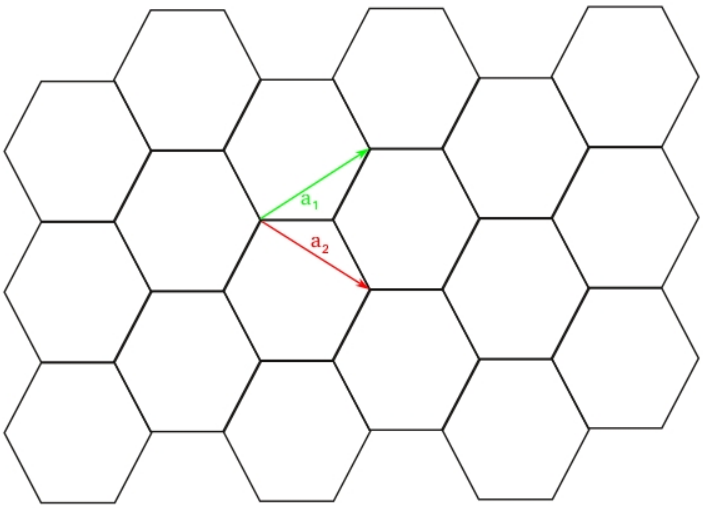

Figure 6.2: The definition of vectors a_1 and a_2 in the hexagonal lattice.

Three types of nanotubes based on the relations of these two numbers can be described.

- armchair nanotube: $m = n$ so then $C_h = (n, n)$
- zig-zag nanotube: $m = 0$ thus $C_h = (n, 0)$
- chiral nanotube: the other possible cases $C_h = (n, m)$

In case of anatase nanotubes it is possible to create 2D sheet which is described by the chiral vector. In Figure 6.3 all 2D sheets of these three types of nanotubes are shown. In our case, the chiral vector $C_h = (8, 8)$ was choosen for armchair nanotube, $C_h = (8, 0)$ for zig-zag nanotube and $C_h = (8, 4)$ for chiral nanotube, respectively.

These 2D sheets are formed to nanotubes by rolling. The rolling direction is along the chiral vector so the axis of the nanotube is perpendicular to the chiral vector and the diameter of the nanotube is given by the length of the chiral vector. These nanotubes are shown in Figure 6.4.

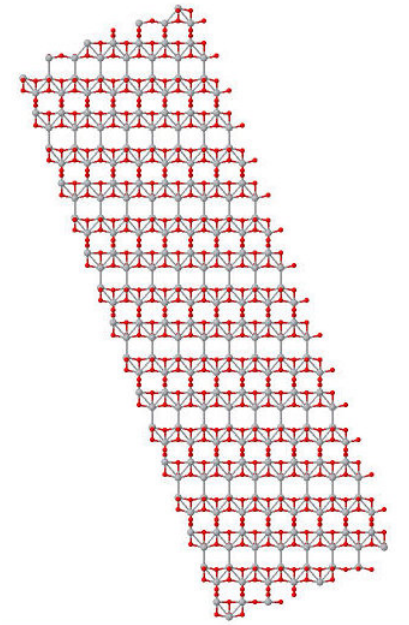

(a) 2D sheet of armchair nanotube

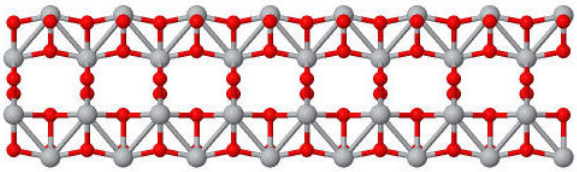

(b) 2D sheet of zig-zag nanotube

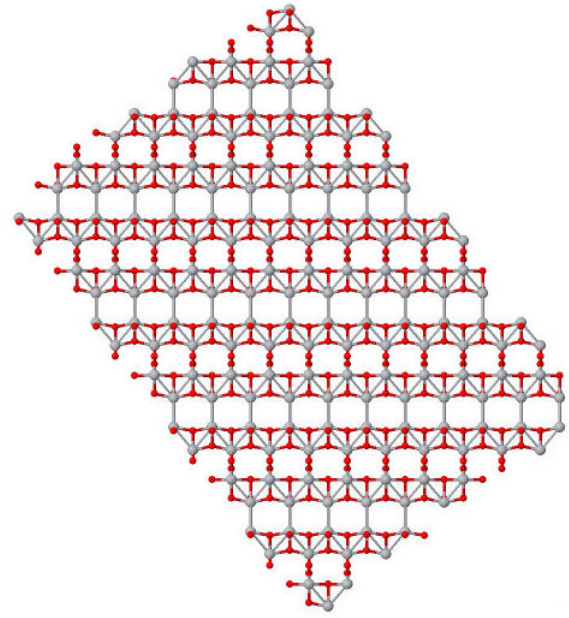

(c) 2D sheet of chiral nanotube

Figure 6.3: 2D sheets of three types of nanotubes (oxygen atoms - red color, titanium atoms - gray color, viewed using Jmol [70]).

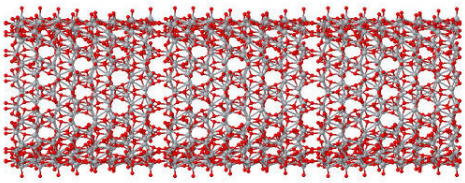

(a) armchair nanotube - side view

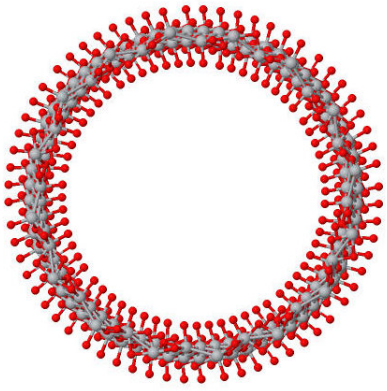

(b) armchair nanotube - top view

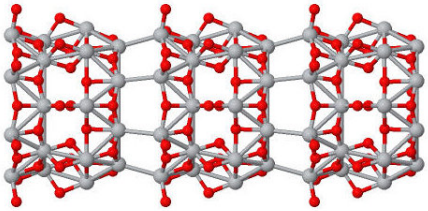

(c) zig-zag nanotube - side view

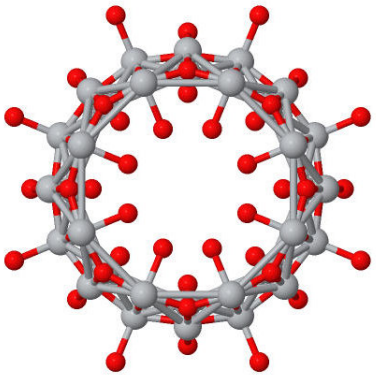

(d) zig-zag nanotube - top view

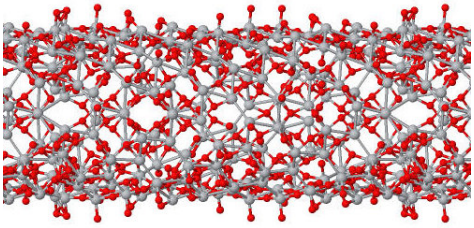

(e) chiral nanotube - side view

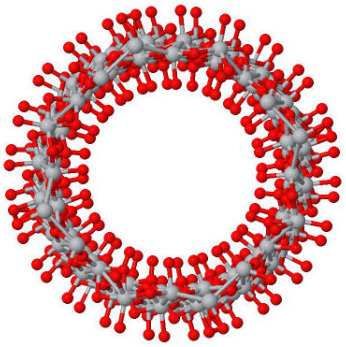

(f) chiral nanotube - top view

Figure 6.4: Three types of anatase nanotubes (oxygen atoms - red color, titanium atoms - gray color, viewed using Jmol [70]).

PXRD patterns were calculated by using these models of nanotubes. The calculations were done with the aid of the Debye formula (3.5). In this chapter, two different samples of Ti-NT were used - prepared from the microcrystalline anatase and the microcristalline rutile, respectively. Measured PXRD patterns from these two samples were found to be almost the same so only one model could be used for description of both samples. However, there exist some subtle differences between them as indicated in Figure 6.5 by green oval. Other differences in the intensity scale could be caused by using not identical amount sample in both measurements.

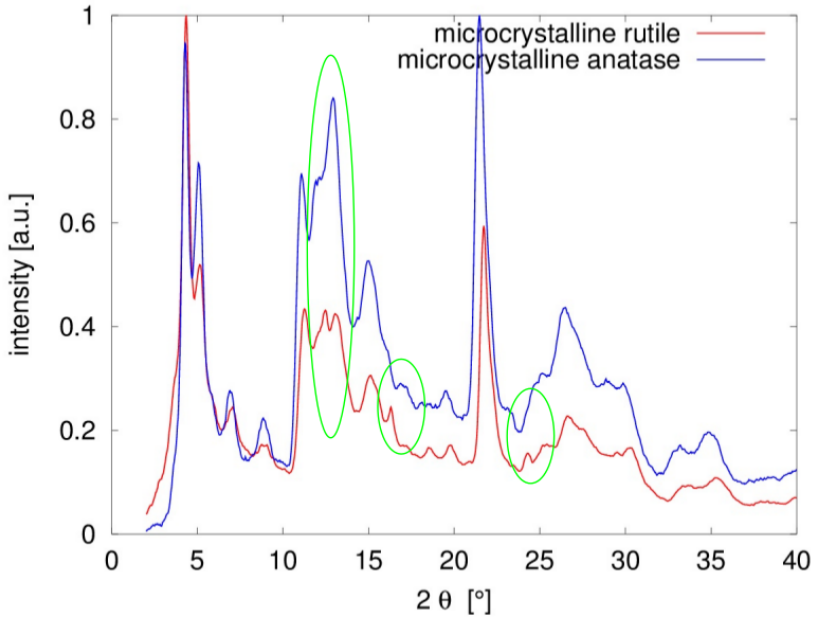

Figure 6.5: Comparison of measured PXRD patterns of Ti-NT prepared from microcrystalline anatase and rutile powders. Green elipses points to different structure in diffraction patterns.

PXRD patterns were measured on Rigaku Rapid II diffractometer with Mo-Kα radiation in transmission geometry as it was described in Chapter 5. Comparison of calculated and measured PXRD patterns is shown in Figure 6.6. As it can be seen, the agreement is quite bad. In case of calculated anatase nanotubes three almost equidistant peaks can be identified in the low angle region of PXRD pattern. These three peaks are not present in the measured PXRD pattern. Furthermore, no matching peaks could be found in comparison (see Figure 6.6). Consequently, we considered another model of nanotubes.

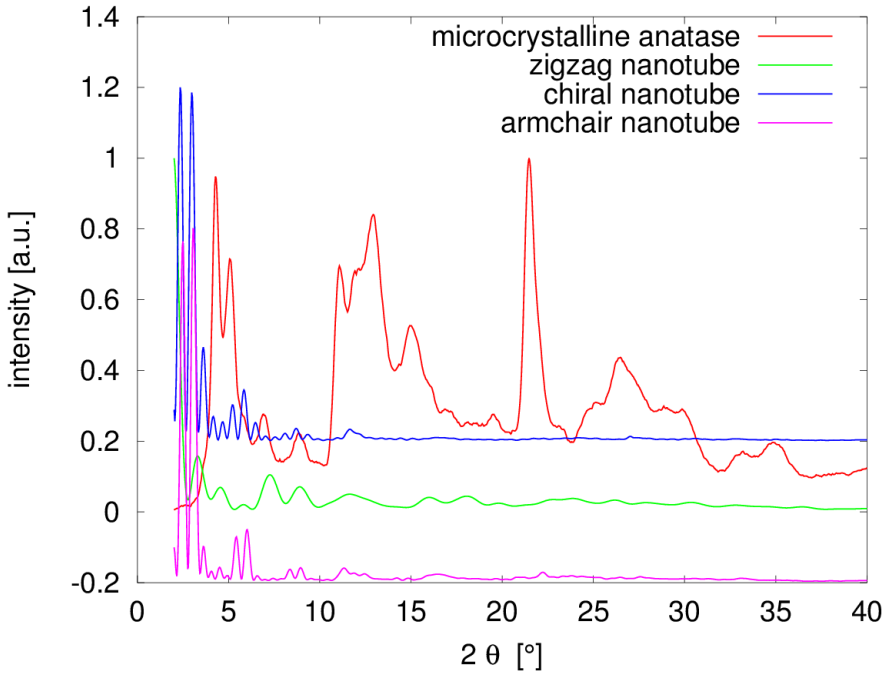

(a) sample prepared from microcrystalline anatase

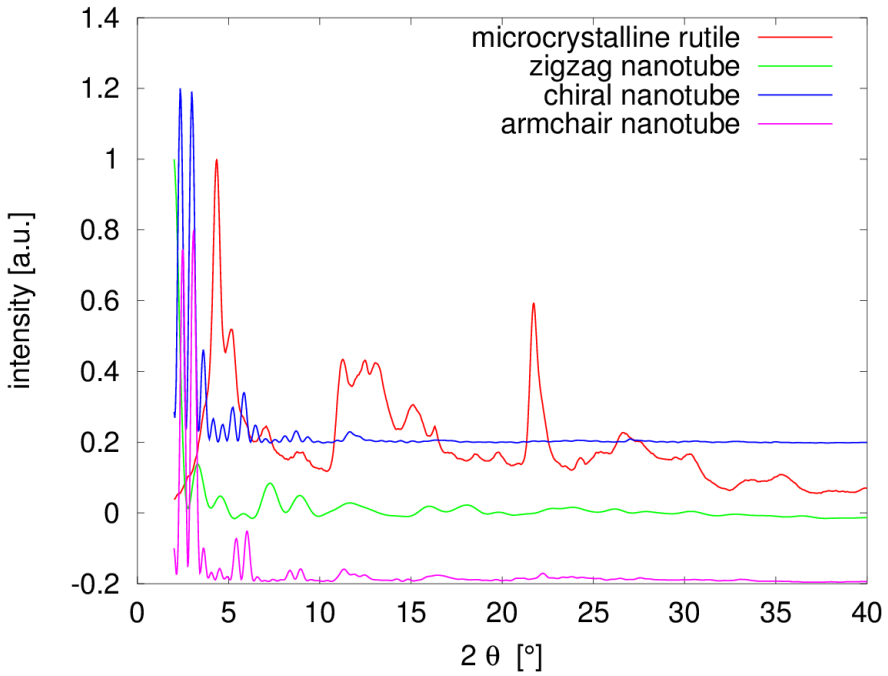

(b) sample prepared from microcrystalline rutile

Figure 6.6: Comparison of PXRD patterns calculated from models of anatase nanotubes and measured PXRD pattern.

6.2. Monoclinic TiO_2 nanotube

The β-TiO_2 was chosen because the model of anatase nanotube did not match well our measured PXRD pattern. Here, the same samples of Ti-NT were used as in the previous section 6.1. The positions of diffraction peaks calculated for this phase taken from the PDF database [59] correspond quite well to the measured pattern. The comparison is shown in Figure 6.7.

β-TiO_2 has monoclinic crystal structure with the lattice parameters [59]:

$$a = 12.1787\,\text{Å},\ b = 3.7412\,\text{Å},\ c = 6.5249\,\text{Å},\ \beta = 107.054^\circ$$

The crystal structure of β-TiO_2 is shown in Attachment 4 in different projections.

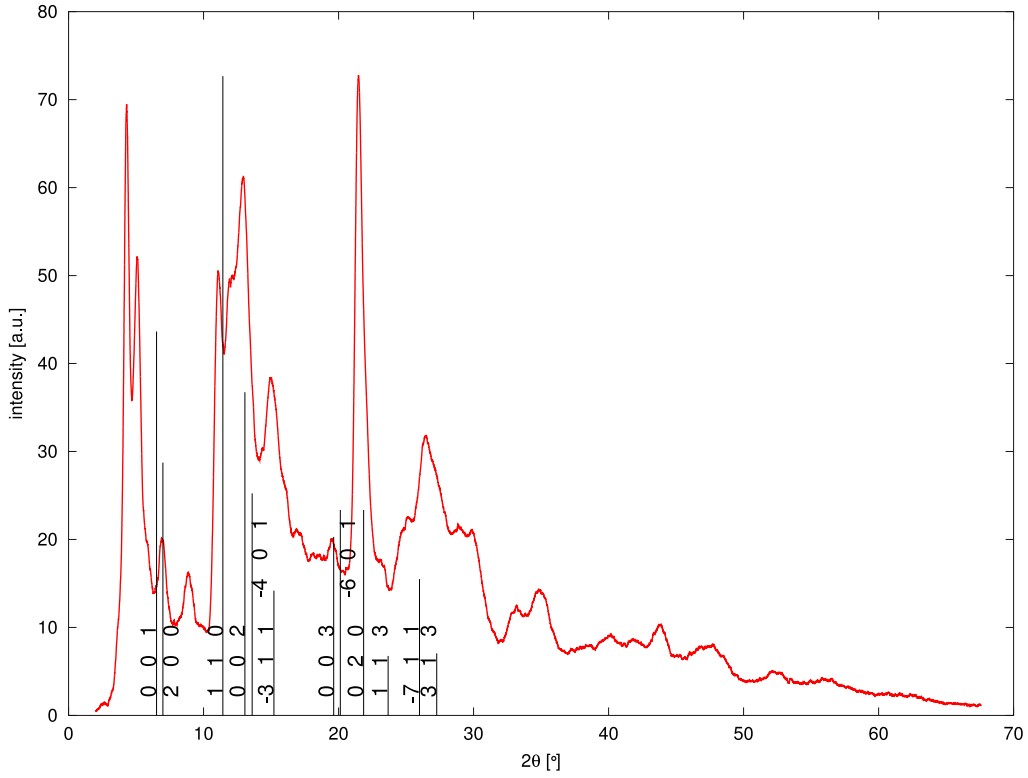

Figure 6.7: Measured PXRD pattern (Mo Kα radiation) of Ti-NT with the indicated positions of diffraction peaks for β-TiO_2 from the database [59].

- Model bulding

  The first step of model building was the creation of a 2D sheet from β-TiO_2 structure. This sheet had special orientation of the monoclinic cell and thickness of this sheet was chosen as a multiplication of one cell parameter. The thickness represents the number of walls of the tube. After that the 2D sheet was rolled into the tube along the chosen axis.

- Orientation of the unit cell in model

  Very sharp peak detected at approximately 22° in 2θ was considered as the diffraction from the long range periodical order of atoms. The longest distance in the nanotube is the length of the tube. From Figure 6.7 it can be seen that the peak corresponds to the 020 reflection. As a result, the nanotube is rolled along the b-axis of monoclinic lattice. The first peak of PXRD pattern usually represents multiwall structure and the c-axis is in the direction of the thickness of 2D sheet.

- Parameters of model

  The orientation of the lattice parameters is the following: b-axis has the same direction as an axis of the nanotube, c-axis has the direction of layers, that means c-axis is pointing to the center of the tube and a-axis is going around circumference and it represent the radius of the nanotube. The parameters of the model are the following: the lattice parameters of monoclinic structure of β-TiO_2 - a, b, c, β and their multiplication factors, not for angle β, of course. In total, seven different parameters were considered in this model. Two of them could be found directly - the lattice parameter b and multiplication of the lattice parameter c. The correct value of the b parameter could be found directly from the position of the mentioned peak at 22° in 2θ. The multiplication of the lattice parameter c corresponds to the number of walls of the nanotube. This could be observed by HRTEM or TEM and it was estimated to the value of 4. PXRD pattern calculated for the nanotube made of the β-TiO_2 just with the lattice parameters taken from the database in comparison with the measured of PXRD pattern of Ti-NT prepared from microcrystalline rutile is shown in Figure 6.8.

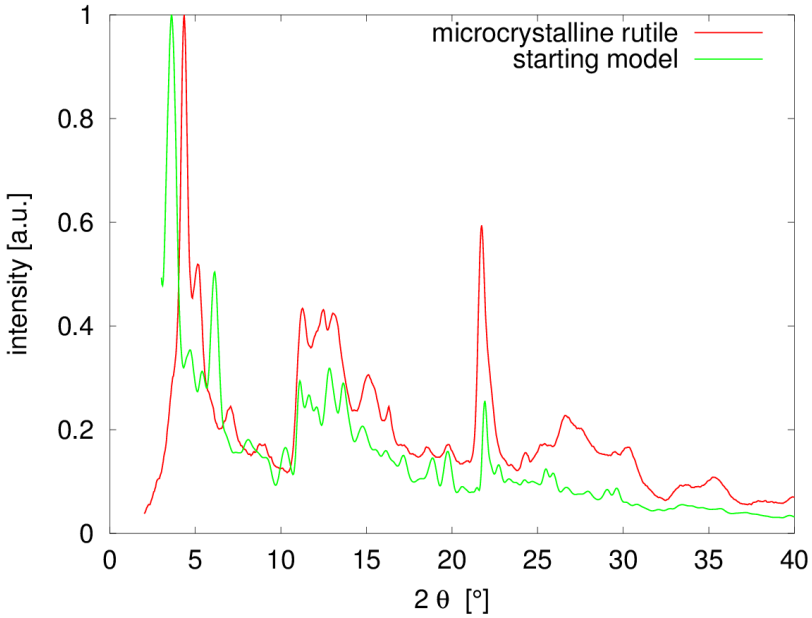

Figure 6.8: PXRD patterns measured for Ti-NT prepared from microcrystalline rutile and calculated for the starting model of Ti-NT.

- Optimization of the model parameters

The other three lattice parameters a, c, β should be found by comparison of the PXRD pattern calculated for different values of these parameters with the experimental data. Two values of each lattice parameter - higher and lower than the value from the database were chosen and used for calculation of PXRD pattern. The changes caused by the variations of the lattice parameters a, c and β are shown in Figures 6.9a, 6.9b and 6.9c, respectively.

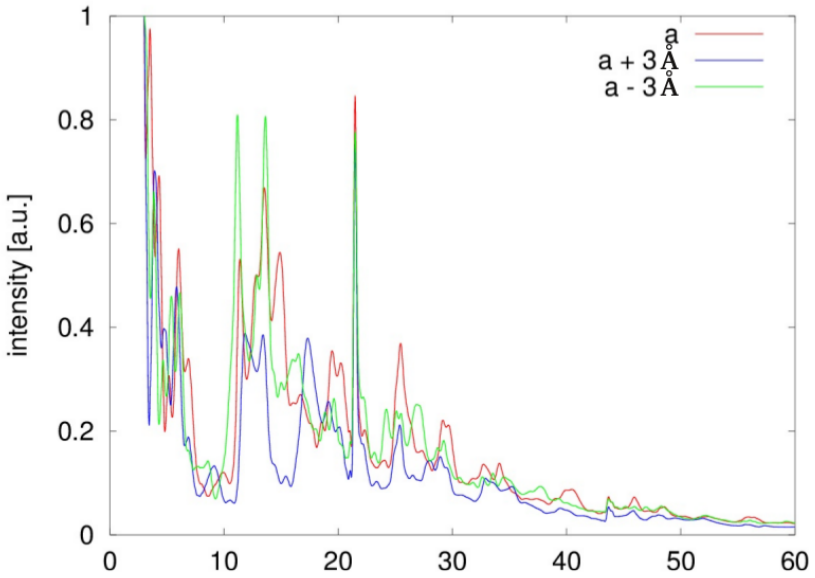

(a) variations of a

Figure 6.9: The changes of PXDR pattern due to variations of the lattice parameters.

In Figures 6.9 some peaks could be indentified which depends on certain lattice parameter but it is really difficult to find some peak which depends only on one lattice parameter. At high diffraction angles there are too many peaks depending on all lattice parameters. Finally, the value of the lattice parameters (a, c, β) were obtained by manual minimization of the least squares (LSM) from a set of the patterns calculated for different values of a, c, β. These values were varied in the intervals shown in Figures 6.9 with steps 0.2 Å and 0.5° for a, c and β, respectively.

For a given set of the lattice parameters, the PXRD patterns were calculated and convoluted with the Gaussian function representing the

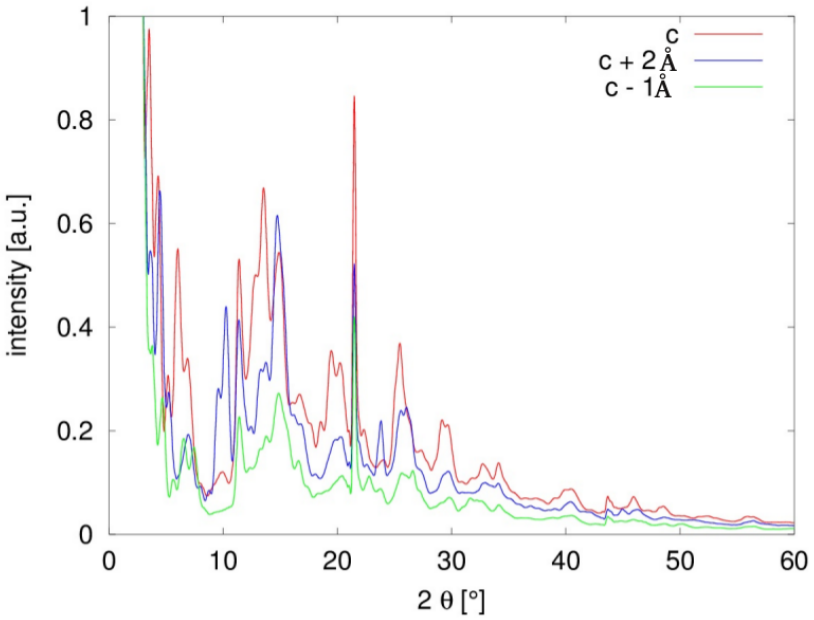

(b) variations of c

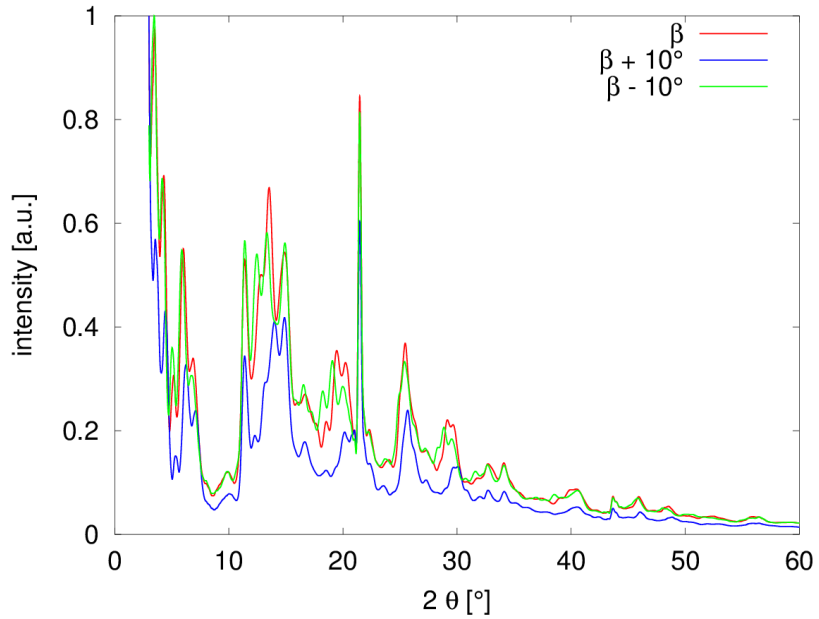

(c) variations of β

Figure 6.9: The changes of PXDR pattern due to variations of the lattice parameters.

instrumental line broadening. The LSM method was applied in the way that always the minimum for two selected lattice parameters was calculated and then one lattice parameter was fixed and for other two parameters the minimum of sum of least squares (SLS) was calculated.

Finally, the multiplication of the lattice parameters a and b should be mentioned. The multiplication of the lattice parameter b corresponds to the length of the nanotube. On TEM images quite long nanotubes were observed, so this multiplicity was chosen as a maximum value which could be seen by X-rays - coherent diffraction length (approximately 1 μm).

The multiplication of the lattice parameter a has an effect only on the diffraction peak to be sharper or blurred. So more discussion is not given about this parameter.

- The results

  The final refined values of lattice parameters obtained by the above method are the following:

$$\text{a} = 14.6\,\text{Å} \quad \text{b} = 3.82\,\text{Å} \quad \text{c} = 5.5\,\text{Å} \quad \beta = 106.1^\circ$$

  for Ti-NT prepared from microcrystalline anatase and

$$\text{a} = 14.6\,\text{Å} \quad \text{b} = 3.77\,\text{Å} \quad \text{c} = 5.3\,\text{Å} \quad \beta = 100.6^\circ$$

  for Ti-NT prepared from microcrystalline rutile, respectively. The final calculated PXRD in comparison with the measured one is shown in Figure 6.10a for Ti-NT prepared from microcrystalline anatase and in Figure 6.10b for Ti-NT prepared from microcrystalline rutile, respectively.

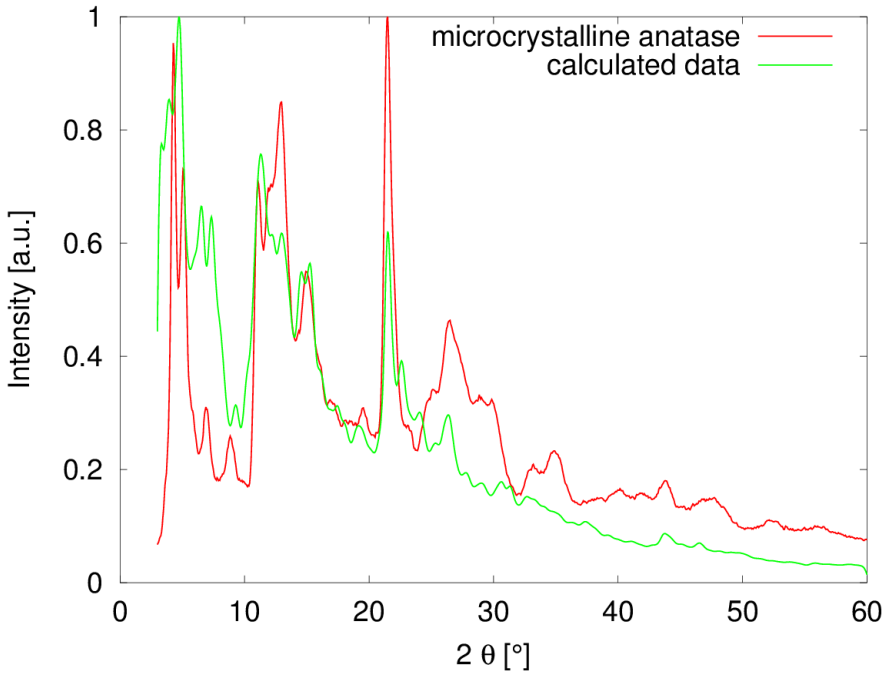

(a) Ti-NT prepared from microcrystalline anatase

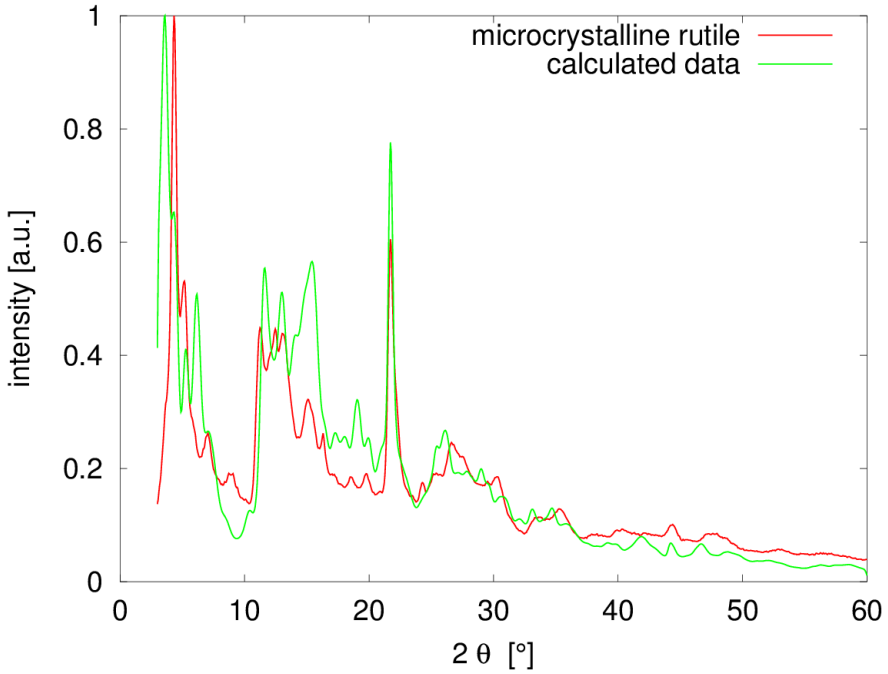

(b) Ti-NT prepared from microcrystalline rutile

Figure 6.10: PXRD pattern calculated with the model parameters obtained by the LSM with the experimental compared with th eexperimental pattern.

6.3. $H_2Ti_2O_5 \cdot H_2O$ nanotube

In spite of quite good agreement between the measured PXRD pattern and the pattern calculated by using the model of monoclinic TiO_2 nanotube it was decided to perform further studies of possible structure of Ti-NT. It should also be mentioned that the agreement was not perfect but only approximate and it could not be improved by variation of the model parameters.

Another series of samples was prepared for structure determination. Each sample was prepared from different initial TiO_2 powder, the grain size and crystal structure were changed as it was mentioned in chapter 4.

EDX analyses reveal Na ions in these samples unlike the previous set. Consequently, the structure of Ti-NT should not be any of structure modification of TiO_2 because if the sodium ions are present titanate salt should be formed. EDX results are shown in Table 6.1. The contents of sodium ions was found in the range of 16 to 24 atomic percents. EDX analysis is not so suitable for the determination of oxygens atoms because they are too light for the method. SEM images were used for study of Ti-NT morfology. Different length of nanotubes prepared from different TiO_2 powder can be seen in Figure 6.11. It is clear that that the nanotubes tend to stick together and there are only bunches of Ti-NT visible. SEM images (Figure 6.11) were colored in order to enhance details and therefore not all SEM images have the same color scheme. More information about the samples could be obtained from the TEM images (Figure 6.12). For example, from different type of contrast it can be decided if nanotubes or nanowires are present in the samples (Figure 6.12c). Figure 6.12 (6.12g) confirms that the nanotubes or nanowires tend to stick together, as it is visible from SEM images (Figure 6.11). Ti-NT prepared from nanorutile seems to be smaller than other samples (see Figure 6.11e).

Table 6.1: EDX results of Ti-NT prepared from different initial powders.

microrutile			
element	nor. C [wt. %]	atom. C [at. %]	error [%]
Titanium K-series	87.07	76.40	2.0
Sodium K-series	12.93	23.60	0.6
nanorutile			
element	nor. C [wt. %]	atom. C [at. %]	error [%]
Titanium K-series	88.69	79.02	2.0
Sodium K-series	11.31	20.98	0.6
microanatase			
element	nor. C [wt. %]	atom. C [at. %]	error [%]
Titanium K-series	88.02	77.93	2.0
Sodium K-series	11.98	22.07	0.6
nanoanatase			
element	nor. C [wt. %]	atom. C [at. %]	error [%]
Titanium K-series	91.21	83.31	2.1
Sodium K-series	8.79	16.69	0.5
brookite			
element	nor. C [wt. %]	atom. C [at. %]	error [%]
Titanium K-series	91.84	84.41	1.9
Sodium K-series	8.16	15.59	0.4

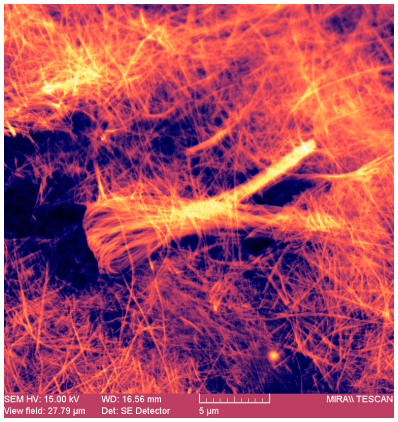

(a) Ti-NT prepared from microrutile (scale 5 μm)

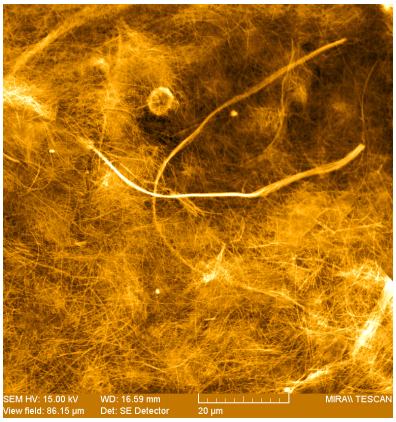

(b) Ti-NT prepared from microrutile (scale 20 μm)

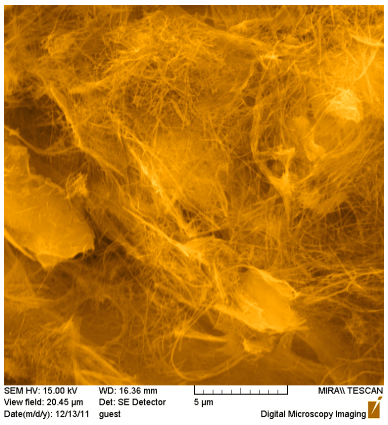

(c) Ti-NT prepared from microanatase (scale 5 μm)

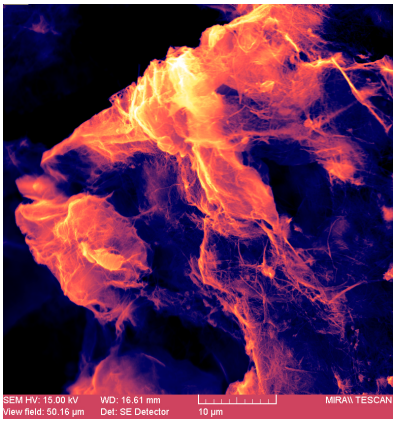

(d) Ti-NT prepared from microanatase (scale 10 μm)

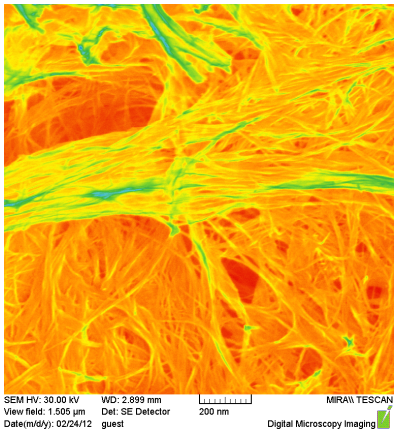

(e) Ti-NT prepared from nanorutile (scale 200 nm)

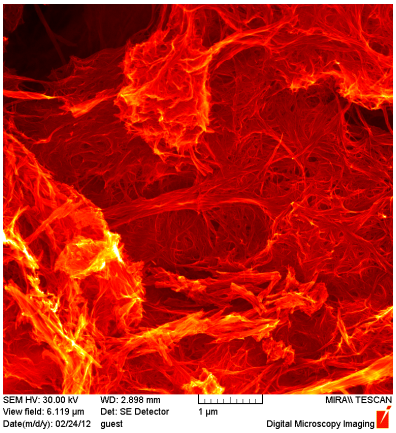

(f) Ti-NT prepared from nanorutile (scale 1 μm)

Figure 6.11: Colored SEM images of Ti-NT.

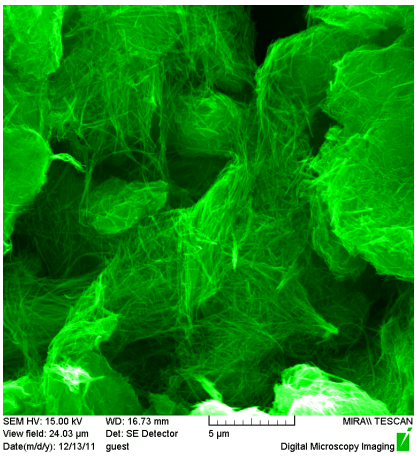

(g) Ti-NT prepared from nanoanatase (scale 5 μm)

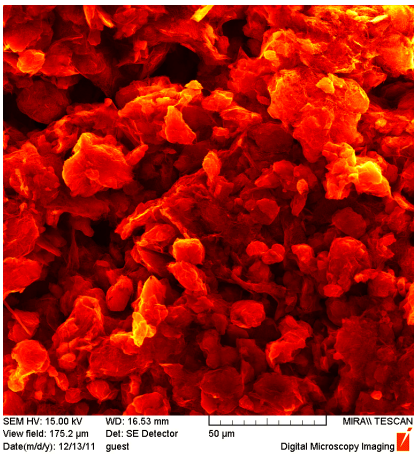

(h) Ti-NT prepared from nanoanatase (scale 50 μm)

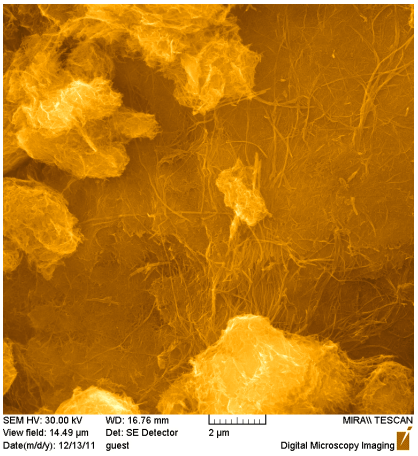

(i) Ti-NT prepared from brookite (scale 2 μm)

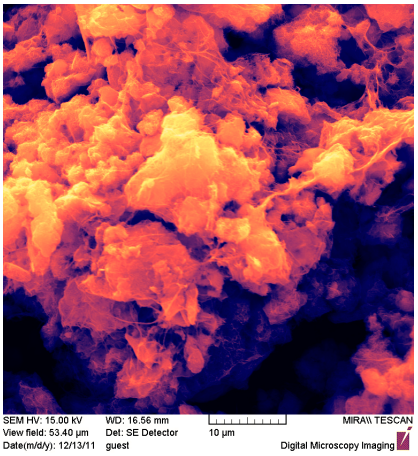

(j) Ti-NT prepared from brookite (scale 10 μm)

Figure 6.11: Colored SEM images of Ti-NT.

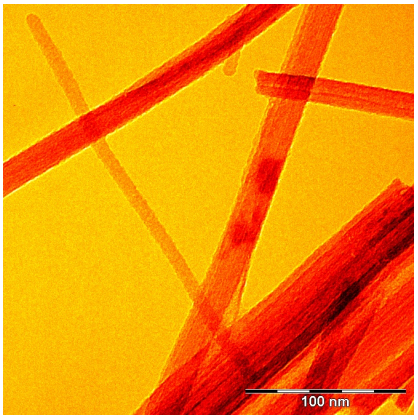

(a) Ti-NT prepared from microrutile (scale 100 nm)

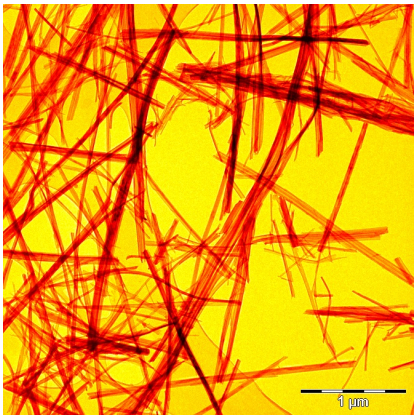

(b) Ti-NT prepared from microrutile (scale 1 μm)

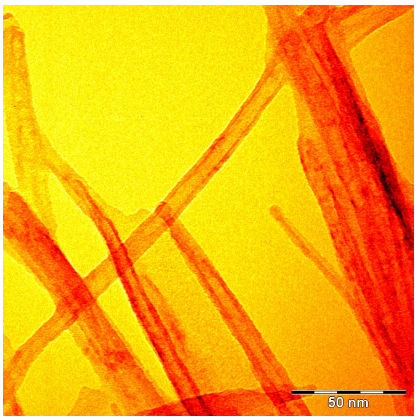

(c) Ti-NT prepared from microanatase (scale 50 nm)

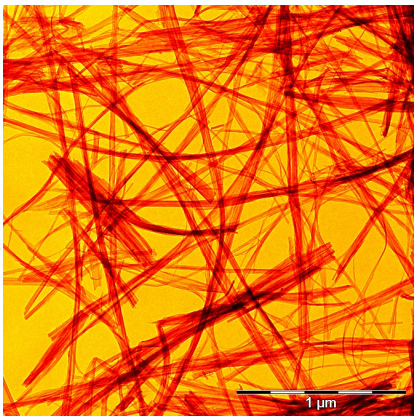

(d) Ti-NT prepared from microanatase (scale 1 μm)

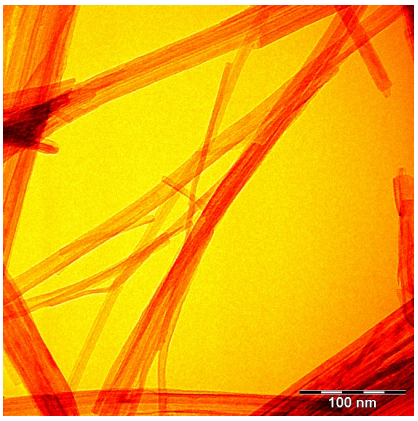

(e) Ti-NT prepared from microanatase (scale 100 nm)

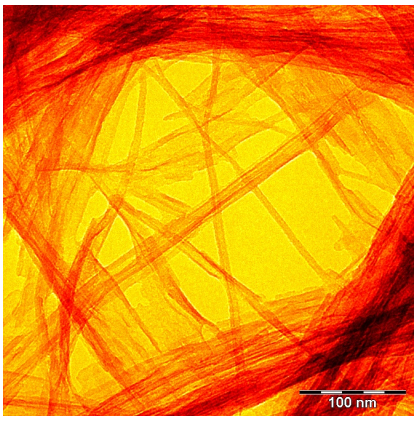

(f) Ti-NT prepared from nanorutile (scale 100 nm)

Figure 6.12: Colored TEM images of Ti-NT.

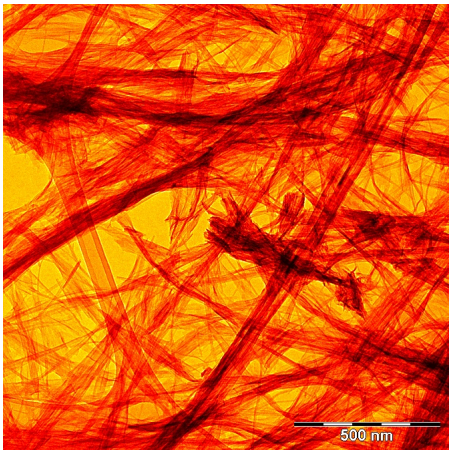

(g) Ti-NT prepared from nanorutile (scale 500 nm)

(h) Ti-NT prepared from nanoanatase (scale 1 μm)

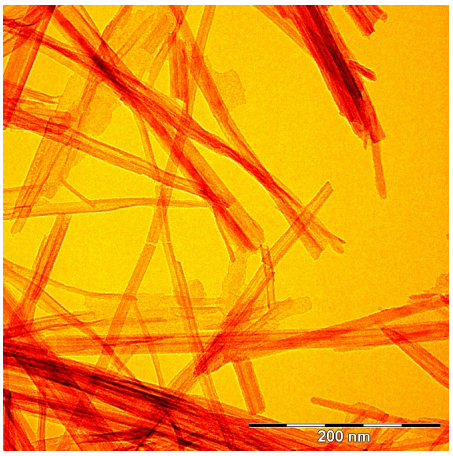

(i) Ti-NT prepared from nanoanatase (scale 200 nm)

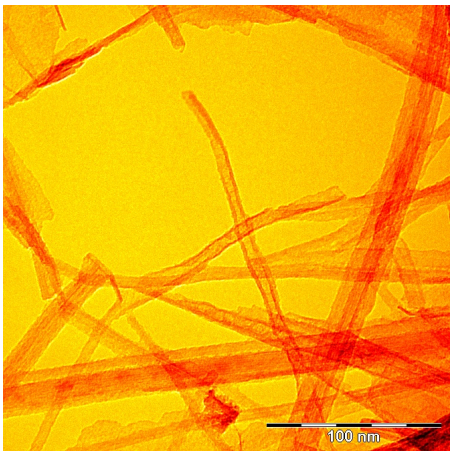

(j) Ti-NT prepared from nanoanatase (scale 100 nm)

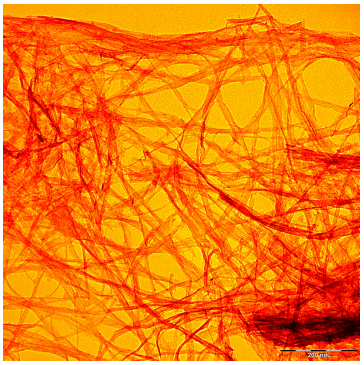

(k) Ti-NT prepared from brookite (scale 200 nm)

Figure 6.12: Colored TEM images of Ti-NT.

The structure of Ti-NT should be one of the titanium salts because the Na ions were detected. In the literature on Ti-NT (chapter 1) some titanium acids (salts) like $H_2Ti_2O_5 \cdot H_2O$ ($Na_2Ti_2O_5 \cdot H_2O$), $H_2Ti_3O_7$ ($Na_2Ti_3O_7$), $H_2Ti_4O_9 \cdot H_2O$ were discussed. The diffraction peak positions taken from the PDF database for these structures are shown in Figure 6.13 together with measured PXRD pattern. In Figure 6.13 only titanium acid is presented because only one titanium salt ($Na_2Ti_3O_7$) can be found in the PDF4 database. The differences between acids and salts can be significant - in case of $H_2Ti_3O_7$ and $Na_2Ti_3O_7$ the differences between peak positions are about 0.7° in 2θ - but with respect to large widths of diffraction lines the diferences between the diffraction patterns of acids and salts could be neglected in the first approximation.

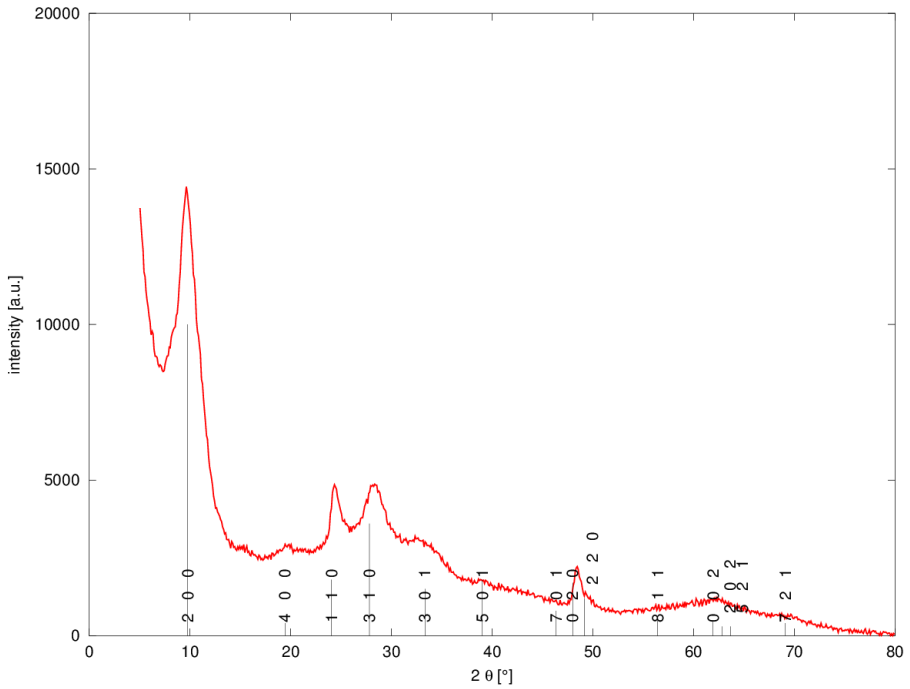

(a) $H_2Ti_2O_5 \cdot H_2O$ [61]

Figure 6.13: PXRD pattern for the Ti-NT prepared from microcrystalline anatase with indicated peak positions of titanium acids taken from the PDF database.

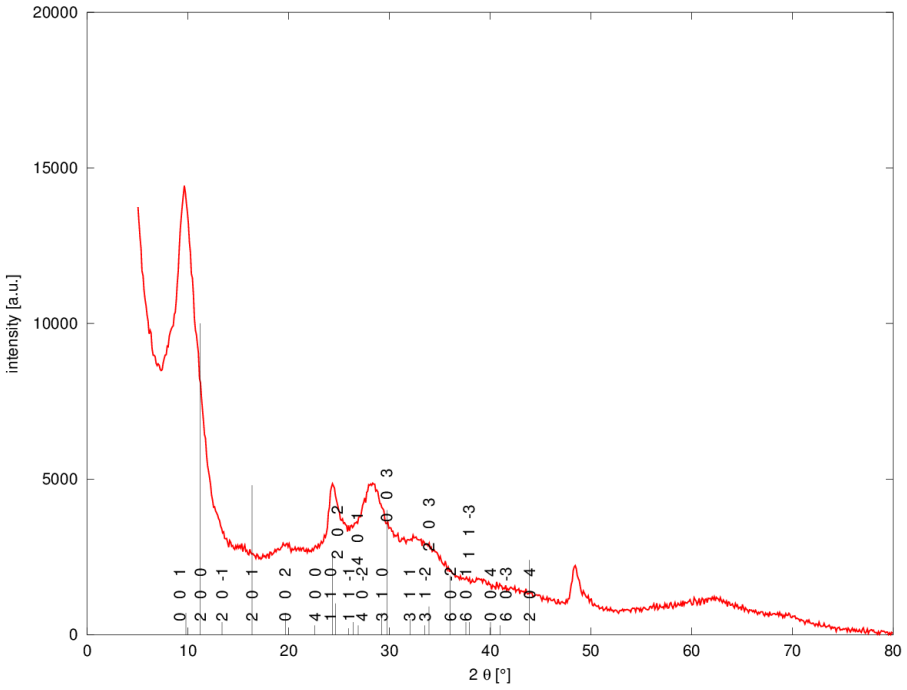

(b) $H_2Ti_3O_7$ [60]

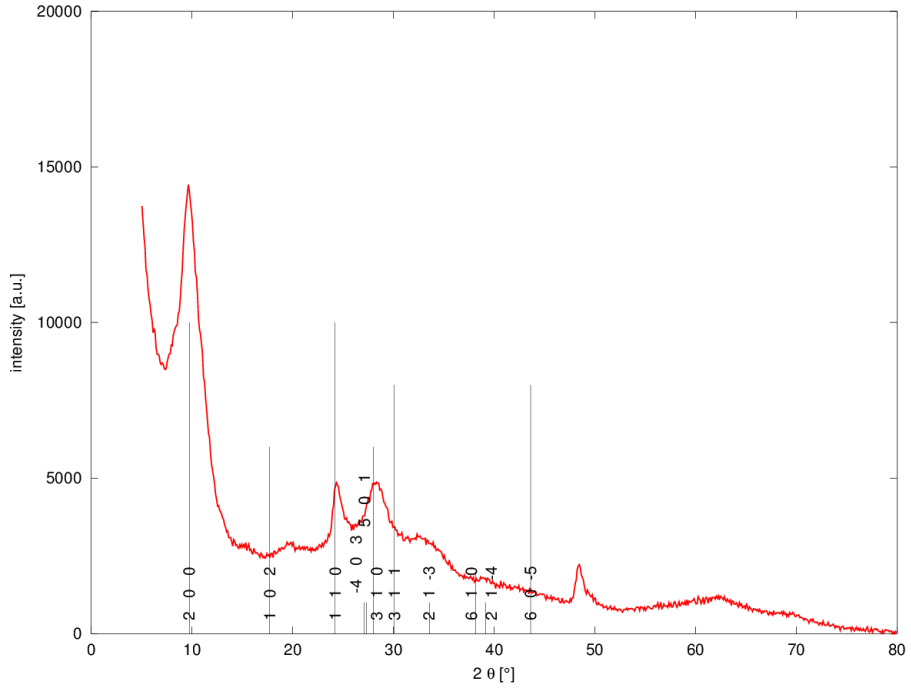

(c) $H_2Ti_4O_9 \cdot H_2O$ [63]

Figure 6.13: PXRD pattern for the Ti-NT prepared from microcrystalline anatase with indicated peak positions of titanium acids taken from the PDF database.

In this part, CuKα radiation was used for all the X-ray measurement. For comparisons with these structures only one of the measured PXRD patterns of Ti-NT was selected - Ti-NT prepared from nanocrystalline anatase. This was the only sample for which we obtained good HRTEM pictures. The reason was that these nanotubes could be well separated one from another and moreover the nanotubes were well dominating in the sample. On the other hand, the sample preparated from microcrystalline rutile contained mainly nanowires and nanotubes were hardly found in HRTEM images. In the sample prepared from nanocrystalline rutile the nanotubes were sticked together and it was impossible to take good HRTEM images for through-focus series method. As a result, the sample prepared from nanocrystaline anatase was utilized for further analysis. Other two samples - prepared from microcrystalline anatase and brookite were not studied by HRTEM.

Comparison of measured PXRD patterns for Ti-NT made from different initial powders is shown in Figure 6.14.

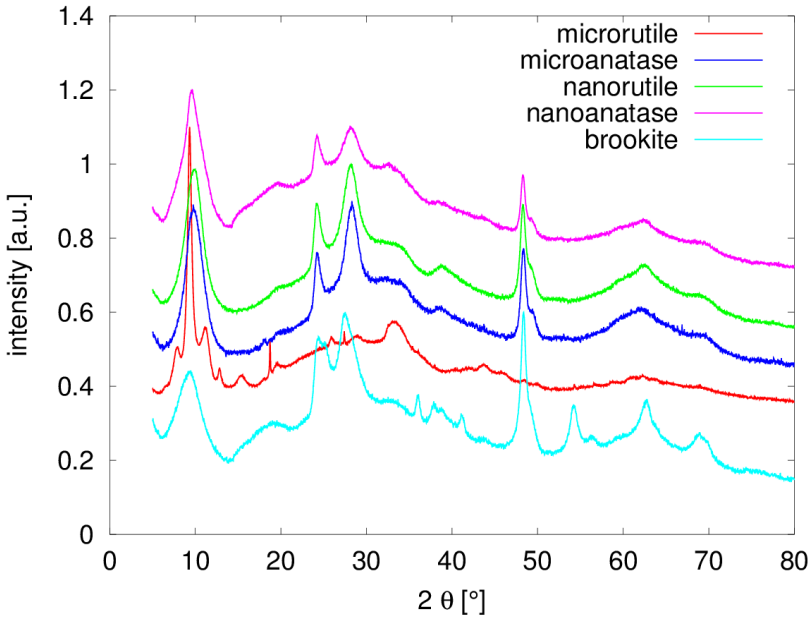

Figure 6.14: PXRD patterns of Ti-NT prepared from different initial powders.

It can be seen that the patterns for samples prepared from microcrystalline anatase, nanocrystalline rutile and nanocrystalline anatase are similar while the pattern for the sample prepared from microcrystalline rutile is quite different. If we look at the pictures obtained by microscopy, it is clear that the latter sample consists mainly of nanowires unlike the others. This probably is a reason for differences in the diffraction patterns. The pattern for sample prepared from brookite is quite similar to those of the former three samples but around $2\theta \sim 35°$ some sharp peaks appeared. Unfortunately, TEM pictures are not available for this sample and it is difficult to estimate if the difference is also related to some fraction on nanowires.

As it can be seen from Figure 6.13 the best match of experimental pattern seems to be with the structure of $H_2Ti_2O_5 \cdot H_2O$ or sodium salt ($Na_2Ti_2O_5 \cdot H_2O$). The structure of $H_2Ti_2O_5 \cdot H_2O$ is the orthorombic with the lattice parameters [61]:

$$a = 18.08\,\text{Å},\ b = 3.797\,\text{Å}, c = 2.998\,\text{Å}$$

In order to verify this assumption the image of the structure of Ti-NT was constructed by through-focus series of HRTEM images of a single nanotube. The principle of through-focus method is based on acquiring twenty HRTEM images with different defocus value. These images were corrected for image shift and then the defocus values of the images were determined. CTF of the images were compensated for and all the corrected images were combined into one structure image. On such image the atoms appear as dark spots (as it was described in chapter 3). The separate images of the through-focus series are shown in Attachment 5. The structure image is presented in Figure 6.15. A 'zig-zag' shape of the edge of nanotube and 'small squares' in the middle of the nanotube are observed in this figure.

Dark dots in the Figure 6.15 represent the Ti-O octahedra. If we enlarge the structure image (Figure 6.15) in the edge and in the middle of the nanotube (Figure 6.16), the lattice parameters can be estimated. Ten dots were measured to obtain the lattice parameters more accurately. Measurements in the edge of the nanotube along the 'zig-zag' shape show the distance of about 38Å. This indicates that one of the lattice parameter of the structure of Ti-NT should be around 3.8 Å. Ten dots in small squares (the middle part of the nanotube) represents approximately 30 Å. Thus the another lattice parameter should be around 3 Å. When we compare these lattice parameters with possible structure suggested from PXRD analysis ($H_2Ti_2O_5 \cdot H_2O$), then the results from HRTEM correspond to the lattice parameters b and c of this structure. As a result it is possible to orient the unit cell in the following way: the axis of the nanotube is along the direction of b-axis and the lattice parameter c is along the circumference of the nanotube.

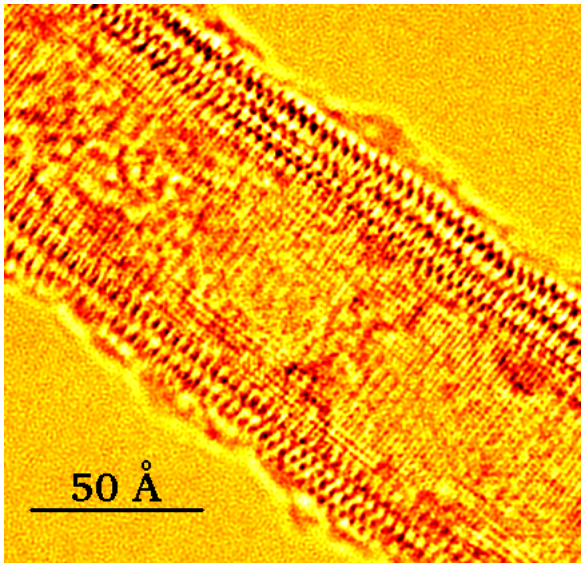

Figure 6.15: The structure image reconstructed from through-focus HRTEM image series.

Owing to the orthorombic lattice of this structure, a-axis is in the direction to the center of the nanotube. The enlarged images of the nanotube is in Figure 6.16. Since we know the orientation of the unit cell in the nanotube now a model of the nanotube can be created.

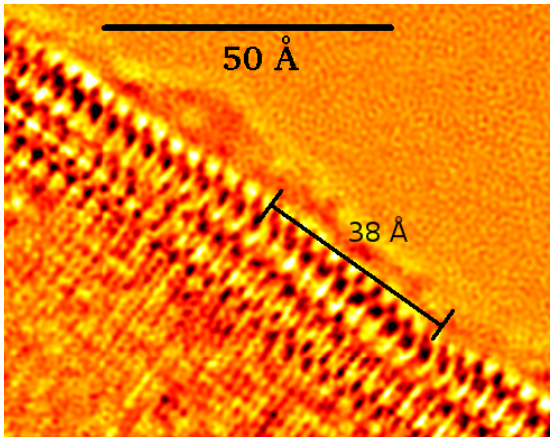

(a) The edge of the nanotube

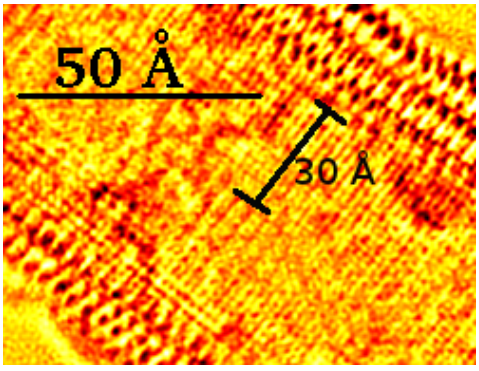

(b) The middle part of the nanotube

Figure 6.16: The enlarged images from HRTEM structure image 6.15.

The important point is that the nanotube has a spiral base. This is visible on Figure 6.15 - on the left side of the nanotube there are only two 'zig-zag' shape lines but three lines can be seen on the right side. We could consider that the nanotube is made by rolling 2D sheet. Unfortunately, the atomic positions in the structure of $H_2Ti_2O_5 \cdot H_2O$ are still unknown. Only the powder pattern has been published so far. Some results were published in the paper [51] but the angle H-O-H in molecule there is around 50° but in water molecule this angle is 109°. Another odd thing in this published atomic positions is a location of two hydrogen atoms very close together which is very unrealistic because of eletric repulsion of the atoms. The projection of this structure is shown in Figure 6.17.

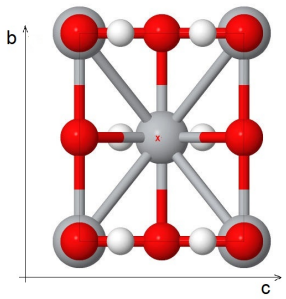

(a) Along a-axis

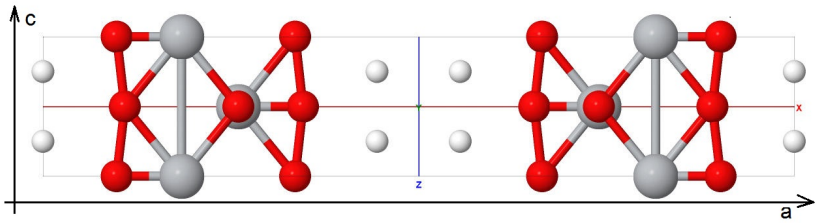

(b) Along b-axis

Figure 6.17: Structure projections of $H_2Ti_2O_5 \cdot H_2O$ in different directions (oxygen atoms - red color, hydrogen atoms - white color, titanium atoms - gray color, viewed using Jmol [70]). Positions of atoms taken from [51].

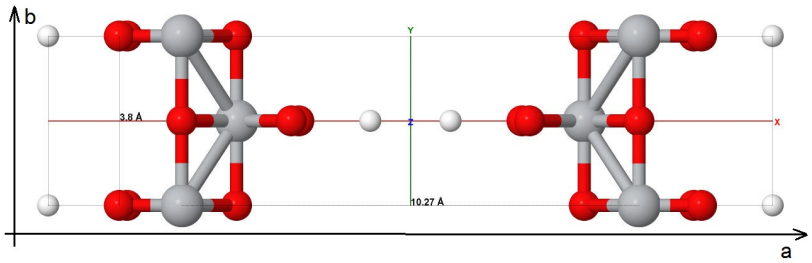

(c) Along c-axis

Figure 6.17: Structure projections of $H_2Ti_2O_5 \cdot H_2O$ in different directions (red ones are oxygen atoms, white ones are hydrogen atoms and gray ones are titanium atoms, viewed using Jmol [70]) possition of atoms from [51].

Consequently, for the creation of a model we had to use another structure with similar lattice parameters and layered Ti-O octahedra. Therefore, we searched PDF4 database for this and we found the phase $(H_3O)_{0.11}Cs_{0.24}Ti_{0.91}O_2(H_2O)_{0.12}$ - orthorombic crystal structure with lattice parameters [79]

$$a = 3.802\,\text{Å},\ b = 1772\,\text{Å}, c = 2.968\,\text{Å}$$

We have used only Ti-O octahedra of this structure for construction of the model of the nanotube. Ti-O octahedra were chosen because this is the main and common building unit in titanates and titanias. The positions of atomic coordinates in z direction of Ti and O atoms were interchanged in order to obtain two titanium atoms per the unit cell. Two parameters must be known for the model: the radius (the diameter of the tube) and the distance between two walls. The diameter of the nanotube could be estimated from the structure image (Figure 6.15). On the other hand the distance between the walls could not be obtained easily from the structure image (Figure 6.15) because it is not well visible. However, the correct value of this parameter can be found from the comparison of calculated and measured PXRD patterns since the first peak of the diffraction pattern depends only on the lattice parameter a which corresponds to the layer of the structure. The model of nanotube in two different orientations is presented in Figure 6.18.

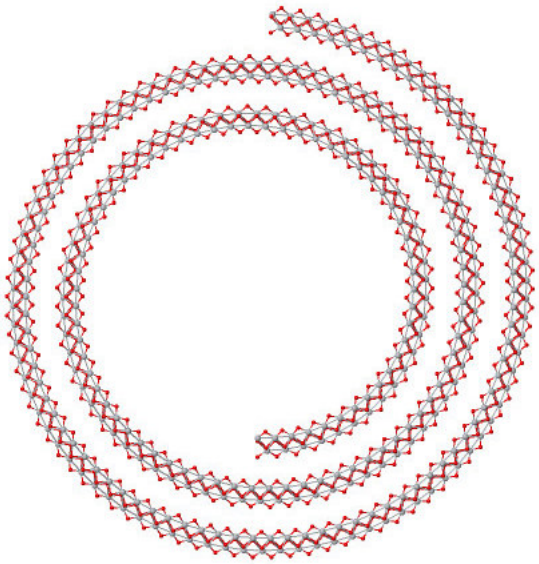

(a) Top view of the tube (visualized by program Jmol [70])

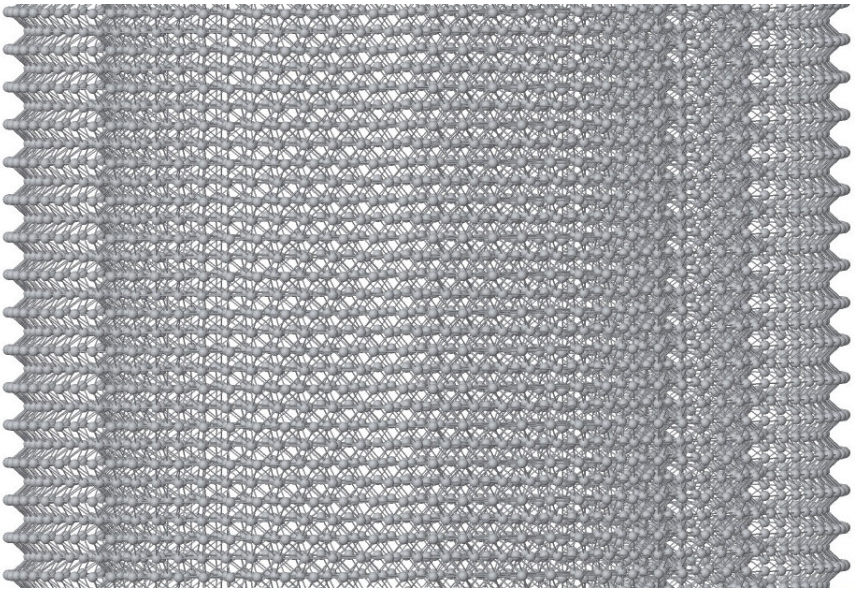

(b) Side view of the tube (visualized by program Jmol [70])

Figure 6.18: Model of the nanotube (oxygen atoms - red, titanium atoms - gray).

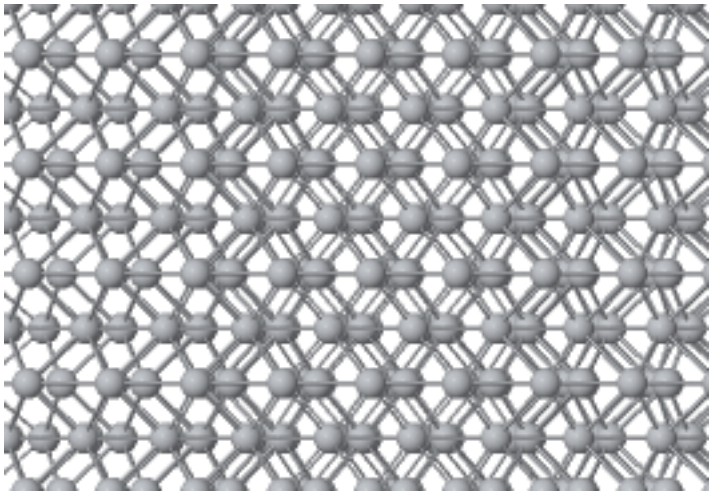

(c) Side view of the tube - detail (visualized by program Jmol [70])

Figure 6.18: Model of the nanotube (oxygen atoms - red, titanium atoms - gray).

Proposed model was used as an input for calculation of PXRD pattern by the Debye formula. Comparison of measured and calculated PXRD patterns is shown in Figure 6.19.

The match of both patterns seems quite good and it is the best result which could be obtained by variation of parameters of the model. One more significant difference can be found at a peak at about 39° of 2θ.

We suggest that this difference could be minimized if preferred orientation of Ti-NT is taken into account. It can be quite understandable that some preferred orientation of the nanotubes can appear during the specimen preparation on glass substrate because the nanotubes would be rather lying on this than standing.

The prefered orientation was preliminary tested on another instrument - horizontal diffractometer PANanalytical MRD with the Eulerioan cradle. The symmetric $\theta - 2\theta$ scans were measured at different inclinations psi of the specimen with respect to the vertical plane (and also the diffracting planes with respect to the substrate plane). In Figure 6.20 these PXRD patterns for Ti-NT prepared from microcrystalline rutile and nanocrystalline anatase are shown. Variations of diffraction peak intensities can clearly be seen. However, the modelling of preferred orientations in calculations with the Debye formula is not a trivial problem and it is a task for future work.

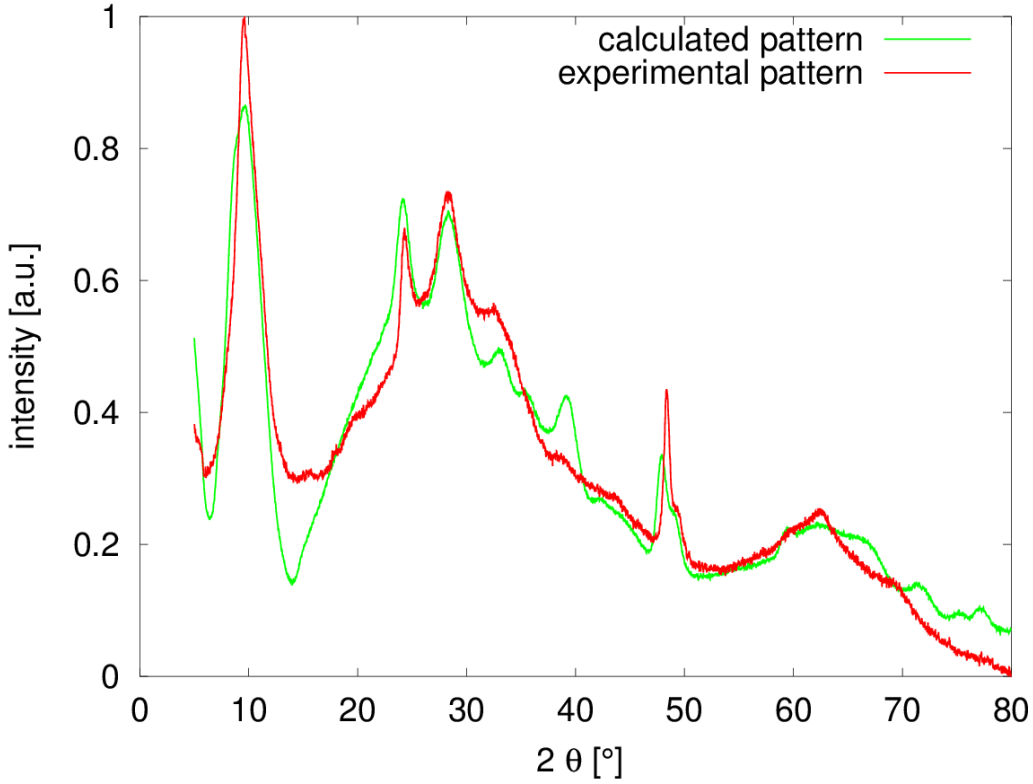

Figure 6.19: The comparison between measure PXRD pattern and measured one.

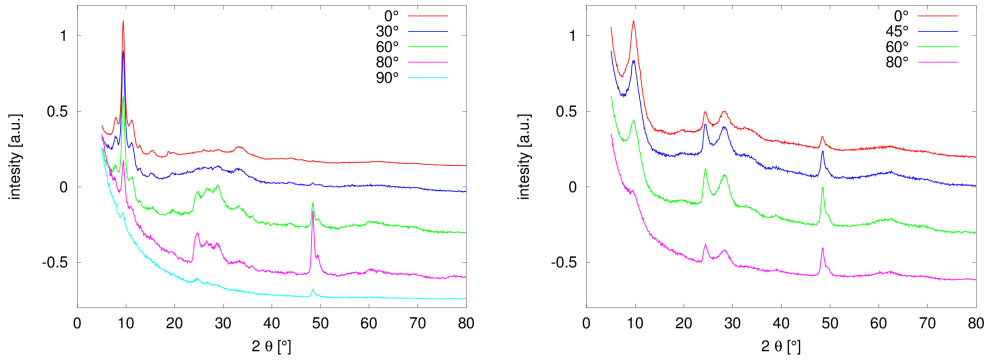

(a) Ti-NT prepared from mikrorutile (b) Ti-NT prepared from nanoanatase

Figure 6.20: PXRD patterns measured at different ψ inclinations.

Finally, it can be concluded that the structure of Ti-NT measured corresponds to that of $Na_xH_{2-x}Ti_2O_5 \cdot H_2O$ phase with the value of x depending on the type of initial TiO_2 powder and washing conditions during praparation. It is given in table (Table 6.2). These values (x) were obtained from EDX results (Table 6.1). The inner diameter of the nanotube is approximately 53.8 Å and the distance between layers is around 9.2 Å, they were obtained from HRTEM images and comparison between measured and calculated PXRD patterns, respectively. This is in good agreement with the published works on Ti-NT (subchapter 1.3).

Table 6.2: Sodium iont concentration in $Na_xH_{2-x}Ti_2O_5 \cdot H_2O$.

	x
microrutile	0.62
nanorutile	0.53
microanatase	0.57
nanoanatase	0.40
brookite	0.37

7. Conclusions

For structure determination of the titanate nanotubes prepared by hydrothermal method mainly two complementary methods were used: X-ray diffraction and transmission electron microscopy. Other methods as energy dispersive X-ray spectroscopy and scanning electron microscopy were used as well.

Three different structural models were constructed in order to determine the structure of Ti-NT. The models were used for the calculations of powder X-ray diffraction patterns with the aid of the Debye formula considering all the atoms in the nanotube. These three models were: anatase nanotube, nanotube created from β-TiO_2 structure and the model based on the structure of $H_2Ti_2O_5 \cdot H_2O$.

The most probable structure of Ti-NT is $Na_xH_{2-x}Ti_2O_5 \cdot H_2O$ where x depends on the preparation powder of Ti-NT and washing condition during preparation. The structure of $H_2Ti_2O_5 \cdot H_2O$ is the orthorombic with the lattice parameters [61]:

$$a = 18.08\,\text{Å},\ b = 3.797\,\text{Å}, c = 2.998\,\text{Å}$$

Nanotube created from this structure was oriented in the following way: the axis of the nanotube is along the direction of b-axis and the lattice parameter c is along the circumference of the nanotube. Owing to the orthorombic lattice of this structure, a-axis is in the direction to the center of the nanotube. The inner diameter of the nanotube is approximately 53.8 Å, determined from through-focus HRTEM images. The distance between layers is around 9.2 Å.

The differences between the structure of Ti-NT prepared from different initial powders was studied on two different series of samples. The first series - Ti-NT prepared from microcrystalline anatase and rutile (discussed in chapter 6.2 and 6.1) had almost the same powder X-ray diffraction patterns that implies they have probably the same structure. On the other hand, the second series (discussed in chapter 6.3) - microcrystalline anatase and rutile, nanocrystalline anatase and rutile, brookite had slightly different powder X-ray diffraction patterns. The differences seem to be caused by the change of the tubular structure to wire structure. This changed structure was observed by HRTEM in samples prepared from nanocrystalline anatase and

microcrystalline rutile. In the sample prepared from microcrystalline rutile any nanotube hardly was seen, there were almost only nanowires there. On the other hand, in the sample prepared from nanocrystalline anatase nanotubes clearly dominated over nanowires.

The morphology of Ti-NT was studied by SEM and TEM. From this studies it was observed that Ti-NT created bundle-like structure where Ti-NT had the length of several microns and they like to stick together.

Bibliography

[1] Iijima S.:. Helical microtubules of graphitic carbon. *Nature*, 354, 1991.

[2] Kasuga T., Hiramatsu M., Hoson A., Sekino T., and Niihara K.:. Formation of titanium oxide nanotube. *Langmuir*, 14, 1998.

[3] http://www.azom.com/article.aspx?ArticleID=1179.

[4] http://automatizace.hw.cz/zajimavost-material-temer-na-vsechno tio2.

[5] http://www.titaniumart.com/photocatalysis ti02.html.

[6] http://www.tio2uk.com/index.htmll.

[7] http://www.tio2.cz/.

[8] http://www.esstech.cz/esstech/eshop/6 1-NANO-TiO2-nastrik.

[9] http://www.ceskatelevize.cz/porady/10121359557-port/tagy/barvy-na-bazi-tio2/369-obrazy-ktere-cisti vzduch/.

[10] http://www.hstrading.co.kr/products/g7.htm.

[11] http://titaniumoxygen.iprostor.cz/solarni-clanky-s tio2.htm.

[12] Bavykin D.V. and Walsh F.C.:. Elongated titanate nanostructures and their applications. *European Journal of Inorganic Chemistry*, 2009.

[13] http://ipc.chem.demokritos.gr/index.php?option=com/content&viev=article&id=303%3Aphoto redox&catid=68%3Aresearchpro&Itemid=11%E2%8C%A9=en.

[14] Idakiev V., Yuan Z.-Y., Tabakova T., and Su B.-L.:. Titanium dioxide nanotubes as supports of nano-sized gold catalysts for low temperature water-gas shift reaction. *Applied catalysis A*, 281, 2005.

[15] Balasundaram G., Yao Ch., and Webster T. J.:. Tio_2 nanotubes functionalized with regions of bone morphogenetic protein-2 increases osteoblast adhesion. *Journal of biomedical materials research part A*, 84A, 2008.

[16] Kasuga T.:. Formation of titanium oxide nanotubes using chemical treatments and their characteristic properties. *Thin solid films*, 496, 2006.

[17] Lopez T., Ortiz-Islas E., Manjarrez J., Reinoso F. R., Sepulveda A., and Gonzalez R. D.:. Biocompatible titania microtubes formed by nanoparticles and its application in the drug delivery of valproic acid. *Optical materials*, 29, 2006.

[18] Lau K.-T., Gu Ch., and Hui D.:. A critical review on nanotube and nanotube/nanoclay related polymer composite materials. *Composites B*, 37, 2006.

[19] Králová D. and et all:. Preparation of gram quantities of high-quality titanate nanotubes and their composites with polyamide 6. *Mater. Chem. Phys.*, 2010.

[20] Poudel B., Wang W. Z., Dames C., Huang J. Y., Kunwar S., Wang D. Z., Banerjee D., Chen G., and Ren Y. F. :. Formation of crystallized titania nanotubes and their transformation into nanowires. *Nanotechnology*, 16, 2005.

[21] Uchida S., Chibe R., Tomiha M., Masaki N., and Shirai M.:. Hydrothermal synthesis of titania nanotube and its application for dye-sensitized solar cell. *Studies in surface science and catalysis*, 146, 2003.

[22] Seo D.-S., Lee J.-K., and Kim H.:. Preparation of nanotube-shaped tio_2 powder. *Journal of crystal growth*, 229, 2001.

[23] Kasuga T., Hiramatsu M., Hoson A., Sekino T., and Niihara K.:. Titania nanotubes prepared by chemical processing. *Advanced Materials*, 11, 1999.

[24] Peng H., Li G., and Zhang Z.:. Synthesis of bundle-like structure of titania nanotubes. *Materials Letters*, 59, 2005.

[25] Wu X., Jiang Q.-Z., Ma Z.-F., FU M., and Shangguan W.-F.:. Synthesis of titania nanotubes by microwave irradiation. *Solid state communications*, 136, 2005.

[26] Zhang Q., Gao L., Sun J., and Zheng S.:. Preparation of long tio_2 nanotubes from ultrafine rutile nanocrystals. *Chemistry Letters*, 2002.

[27] Wang Y. Q., Hu G. Q., Duan X. F., Sun H. L., and Xue Q. K.:. Microstructure and formation mechanism of titanium dioxide nanotubes. *Chemical physics letters*, 365, 2002.

[28] Yao B. D., Chan Y. F., Zhang X. Y., Zhang W. F., Yang Z. Y., and Wang N.:. Formation mechanism of tio$_2$ nanotubes. *Applied physics letters*, 82, 2003.

[29] Wang W., Varghese O. K., Paolose M., Grimes C. A., Wang Q., and Dickey E. C.:. A study on the growth and structure of titania nanotubes. *Journal of Materials Research*, 19, 2004.

[30] Lan Y., Gao X., Zhu H., Zheng Z., Yan T., Wu F., Ringer S. P., and Song D.:. Titanate nanotubes and nanorods prepared from rutile powder. *Advanced functional materials*, 15, 2005.

[31] Deng Q., Wei M., Ding X., Jiang L., Ye B., and Wei K.:. Brookite-type tio$_2$ nanotube. *Chemical communication*, 2008.

[32] Armstrong G., Armstrong A. R., Canales J., and Bruce P. G.:. Nanotubes with the tio$_2$-b structure. *Chemical communication*, 2005.

[33] Sutrisno H. :. Synthesis and characterization of tio$_2$(b) nanotubes prepared by hydrothermal method using [ti$_8$o$_{12}$(h$_2$o)$_{24}$cl$_8$hcl·7h$_2$o as precursor. *Makara, Sains*, 14, 2010.

[34] Pradham S. K., Mao Y., Wong S. S., Chlupas P., and Petkov V.:. Atomic-scale structure of nanosized titania and titanate: particles, wires and tubes. *Chemistry of materials*, 19, 2007.

[35] Kim G.-S., Godbole V. P., Seo H.-K., Kim Y.-S., and Shin H.-K.:. Sodium removal from titanate nanotubes in electrodeposition process. *Electrochemistry communications*, 8, 2006.

[36] Zhu K. R., Yuan Y., Zhang M. S., Hong J. M., Deng Y., and Yin Z.:. Structural transformation from nahti$_3$o$_7$ nanotube to na$_2$ti$_6$o$_1$3 nanorod. *Solid state communications*, 144, 2007.

[37] Yoshida R., Suzuki Y., and Yoshikawa S.:. Effects of synthestic conditions and heat-treatment on the structure of partially ion-exchange titanate nanotube. *Materials chemistry and physics*, 91, 2005.

[38] Bavykin D. V., Parmon V.N., Lapkin A. A., and Walsh F.C.:. The effect of hydrothermal conditions o the mesoporous structure of tio$_2$ nanotubes. *Journal of materials chemistry*, 14, 2004.

[39] Du G.H., Chen Q., Che R.C., Yuan Z. Y., and Peng L.-M.:. Preparation and structure analysis of titanium dioxide nanotube. *Applied physics letters*, 79, 2001.

[40] Yuan Z.-Y. nd Su B.-L.:. Titanium dioxide nanotubes, nanofibers and nanowires. *Colloids and surfaces A*, 241, 2004.

[41] Ma R., Fukuda K., Sasaki T., Osada M., and Bando Y.:. Structural features of titanate nanotubes/nanobelts revealed by raman, x-ray absorption fine structure and electron diffraction. *Journal of physical chemistry B*, 109, 2005.

[42] Ma R., Bando Y., and Sasaki T.:. Nanotubes of lepidocrocite titanates. *Chemical physics letters*, 380, 2003.

[43] Suzuki Y. and Yoshikawa S.:. Synthesis and thermal analysis of TiO_2-derived nanotubes prepared by the hydrothermal method. *Journal of Materials Research*, 19, 2004.

[44] Morgado E. jr, de Abreu M.A.S., Pravia O.R.C., Marinkovic B.A, Jardim P.M., Rizzo R. C., and Arajo A.S.:. A study on the structure and thermal stability of titanate nanotubes as a function of sodium content. *Solid State Science*, 8, 2006.

[45] Morgado E. Jr., de Abreu M.A.S., Moure G.T., Marinkovic B. A., Jardim P. M., and Araujo A. S.:. Characteriztion of nanostrucured titanates obtained by alkali treatment of tio_2-anatases with distinct crystal shape. *Chemistry of Materials*, 19, 2007.

[46] Thorne A., Kruth A., Tunstall D., Irvine J. T. S., and Zhou W.:. Formation, structure and stability of titanate nanotubes and their proton conductivity. *Journal of physical chemistry B*, 109, 2005.

[47] Kubota Y., Kurata H., and Isoda S.:. Nanodifraction and characterization of titanate nanotube prepared by hydrothermal method. *Molecular crystals & Liquid crystals*, 445, 2006.

[48] Yang J., Jin Z., Wang X., Li W., Zhang J., Zhang S., Guo X., and Zhang Z.:. Study on composition, structure and formation process of nanotube $Na_2Ti_2O_4(OH)_2$. *Dalton*, 2003.

[49] Zhang M., Jin Z., Zhang J., Yang J. Guo X., Li W., Wang X., and Zhang Z.:. Effect of annealing temperature on morphology, structure and photocatalytic behavior of nanotubed $H_2Ti_2O_4(OH)_2$. *Journal of Molecular Catalyst A,*, 217, 2004.

[50] Tsai Ch.-Ch., Nian J.-N., and Teng H.:. Mesoporous nanotube aggregates obtained from hydrothermally treating tio_2 with naoh. *Applied surface science*, 253, 2006.

[51] Tsai T.-T. and Teng H.:. Structural features of nanotubes synthesized from naoh treatment on tio_2 with different post-treatmentss. *Chemistry of Materials*, 18, 2006.

[52] Chen W., Gou X., Zhang S., and Jin Z.:. Tem study on the formation mechanism of sodium titante nanotubes. *Journal of Nanoparticle Research*, 9, 2007.

[53] Xu Y., Fang X., Xiong J., and Zhang Z.:. Hydrothermal transformation of titanate nanotubes into single-crystalline tio_2 nanomaterials with controlled phase composition and morphology. *Materials research bulletin*, 45, 2010.

[54] Kochkar H., Lakhdhar N., Berhault G., Bausach M., and Ghorbel A.:. Optimization of the alkaline hydrothermal route to titanate nanotubes by a doehlert matrix experience design. *Journal of physical chemistry C*, 113, 2009.

[55] Yan Y., Qiu X., Wang H., Li L., Fu X., Wu L., and Li G.:. Synthesis of titanate/anatase composites with highly photocatalytic decolorization of dye under visible light irradiation. *Journal of alloys and comnpounds*, 460, 2008.

[56] Nakahira A., Kato W., Tamai M., Isshiki T., and Nishio K.:. Synthesis of nanotube from a layered $H_2Ti_4O_9$ H_2O in a hydrothermal treatment using various titania sources. *Journal of materials science*, 39, 2004.

[57] PDF4 data based. card number 00-021-1272.

[58] PDF4 data based. card number 00-029-1360.

[59] PDF2 data based. card number 74-1940.

[60] PDF4 data based. card number 00-047-0561.

[61] PDF4 data based. card number 00-047-0124.

[62] PDF4 data based. card number 00-057-0123.

[63] PDF4 data based. card number 00-036-0655.

[64] Zou X., Hovmller S., and Oleynikov P.:. *Electron crystalography, Electron microskopy and electron difraction*. Oxford, 2011.

[65] Dinnebier R.E. and Billinge S.J.L., editors. *Powder Diffraction, Theory and Practise*. RSC Publishing, 2008.

[66] Valvoda V., Polcarová M., and Lukač P.:. *Základy strukturní analýzy*. Karolinum, 1992.

[67] Warren B.E.:. *X-ray diffraction*. Dover publications, 1990.

[68] http://physics.mff.cuni.cz/vyuka/zfp/418a.pdf.

[69] PDF4 data based. card number 00-021-1276.

[70] Jmol. http://www.jmol.org/.

[71] Králová D., Pavlova E., Šlouf M., and Kužel R.:. Preparation and structure of titanate nanotubes. *Materials Structure*, 15(1), 2008.

[72] Králová D., Šlouf M., and Kužel R.:. Synthezis of titanate nanotubes: Influence of TiO_2 modification on crystallinestructure and morphology. *Materials Structure*, 15(2a), 2008.

[73] Chen Q., Zhou W., Du G., and Peng L.-M.:. Trititanate nanotubes made via a single alkali treatment. *Advanced materials*, 14, 2002.

[74] Enyashin A. N and Seifert G.:. Structure, stability and electronic properties of tio_2 nanostructures. *Physica status solidi(b)*, 242, 2005.

[75] Ma R., Bando Y., and Sasaki T.:. Directly rolling nanosheets into nanotubes. *Journal of physical chemistry B*, 108, 2004.

[76] Zhang S., Chen Q., and Peng L.-M.:. Structure and formation of $h_2ti_3o_7$ nanotubes in alkali environment. *Physical review B*, 71, 2005.

[77] Ivanovskaya V.V., Enyashin A.N., Medvedeva N. I., and Ivanovskii A. L.:. Electronic proprties of tio_2 nanotubes. *arXiv:cond-mat/0211441v1*, 2002.

[78] Saito R., Dresselhaus G., and Dresselhaus M.S.:. *Physical properties of carbon nanotubes*. Imperial College Press, 1998.

[79] PDF4 data based. card number 04-011-1868.

List of tables

Abbreviations

1D	.....	one-dimensional
2D	.....	two-dimensional
3D	.....	three-dimensional
BB	.....	Bragg-Brentano geometry
CTF	.....	contrast transfer function
EDX	.....	X-ray energy dispersive spectroscopy
EM	.....	electron microscopy
FEG	.....	field emission gun
HRTEM	.....	high resolution transmission electron microscopy
LSM	.....	least square method
PXRD	.....	powder X-ray diffraction
SEM	.....	scanning electron microscopy
SLS	.....	sum of least squares
TEM	.....	transmission electron microscopy
Ti-NT	.....	titania or titanate nanotubes
XRD	.....	X-ray diffraction

List of attachments

Attachment 1

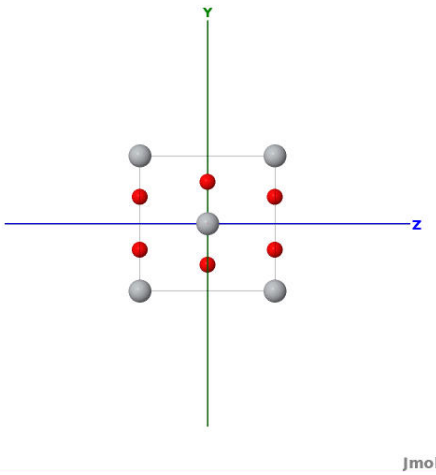

(a) projection along a-axis

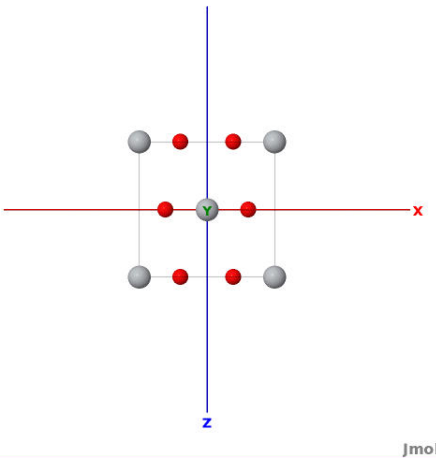

(b) projection along b-axis

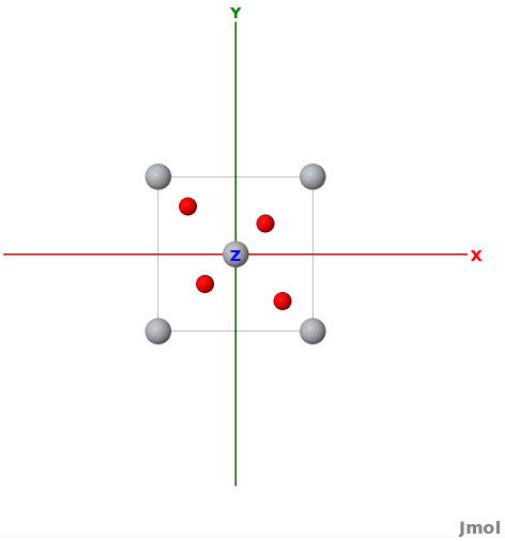

(c) projection along c-axis

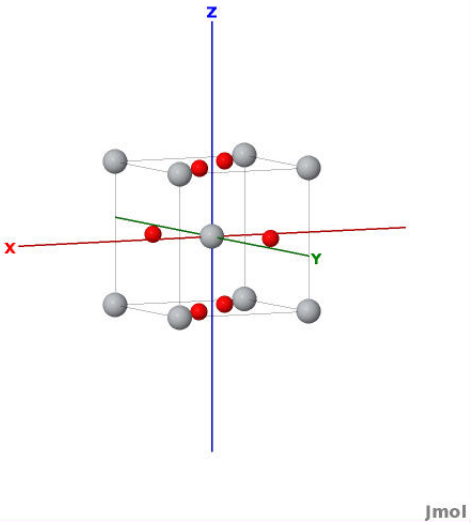

(d) view to the unit cell

The scrystal structure of the rutile (gray atoms are titanium atoms and red ones are oxygens atoms) [70].

Attachment 2

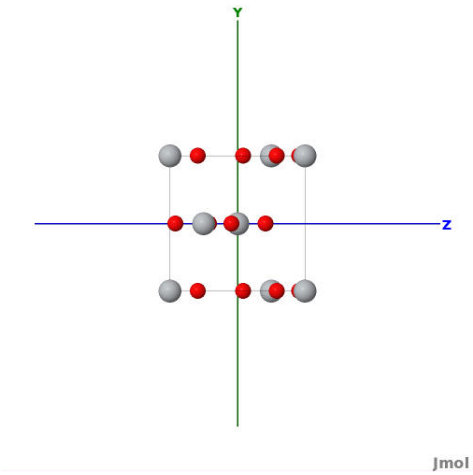

(a) projection along a-axis

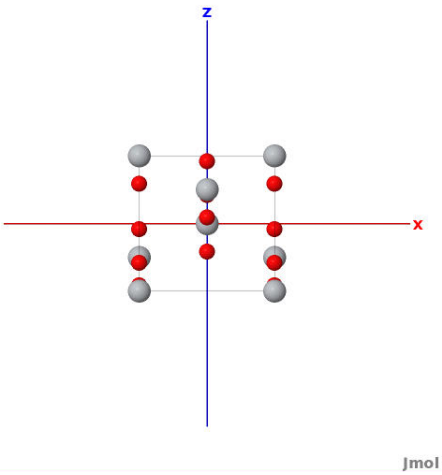

(b) projection along b-axis

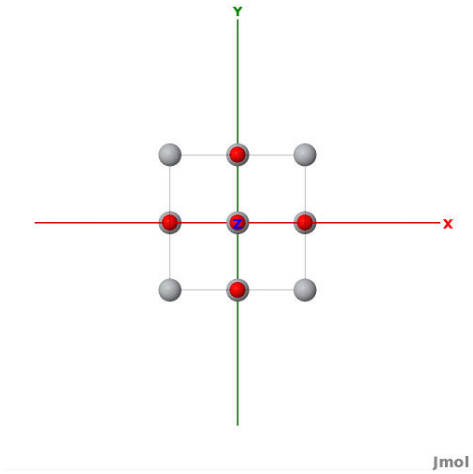

(c) projection along c-axis

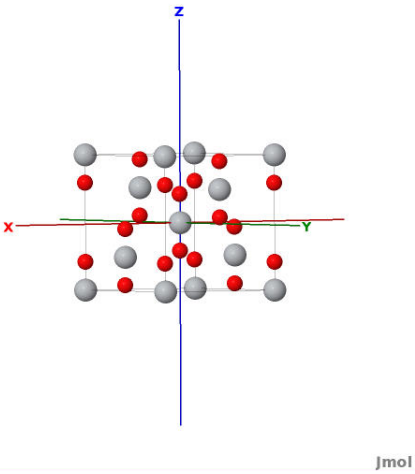

(d) view to the unit cell

The scrystal structure of the anatase (gray atoms are titanium atoms and red ones are oxygens atoms) [70].

Attachment 3

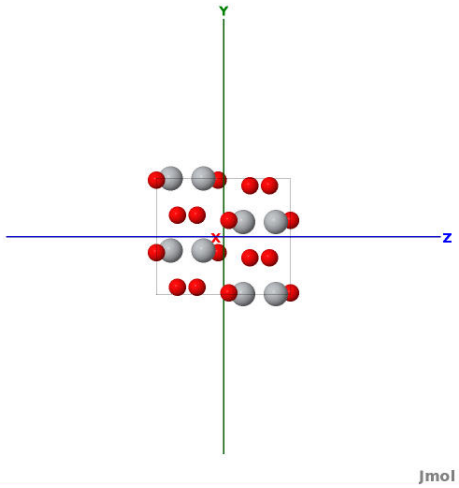

(a) projection along a-axis

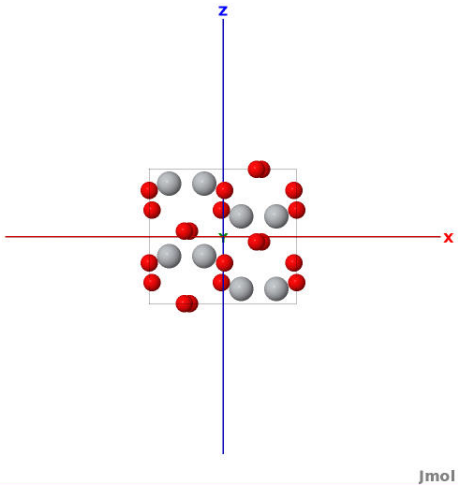

(b) projection along b-axis

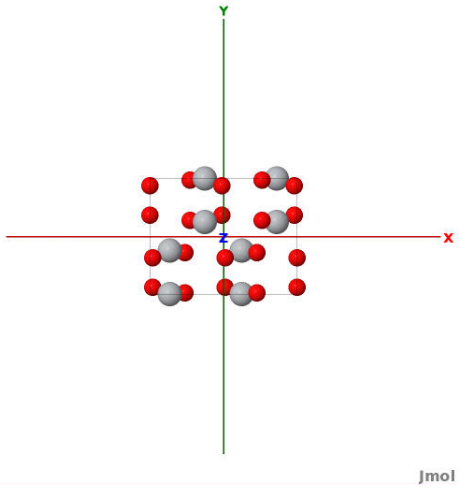

(c) projection along c-axis

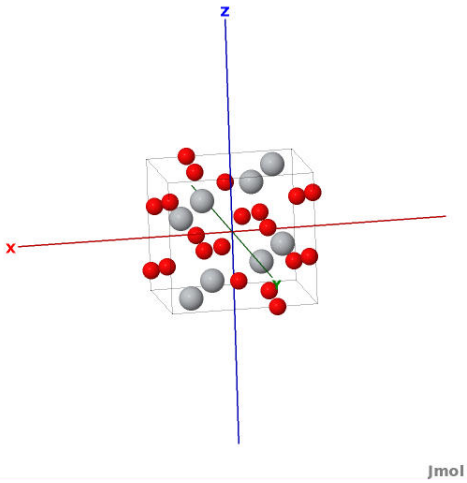

(d) view to the unit cell

The scrystal structure of the brookite (gray atoms are titanium atoms and red ones are oxygens atoms) [70].

Attachment 4

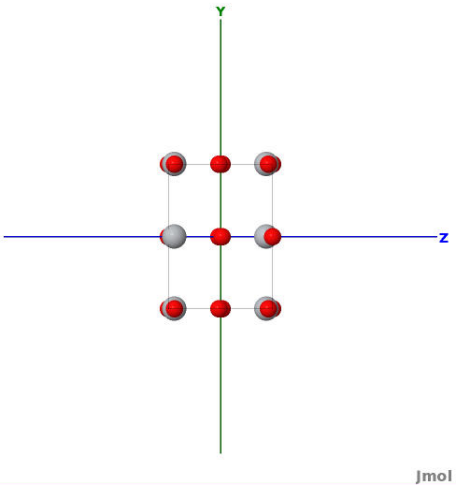

(a) Projection along a-axis

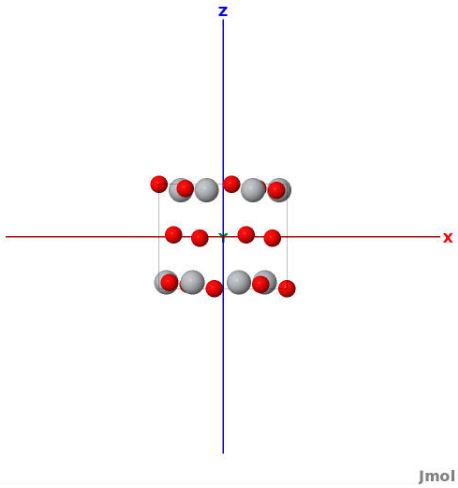

(b) Projection along b-axis

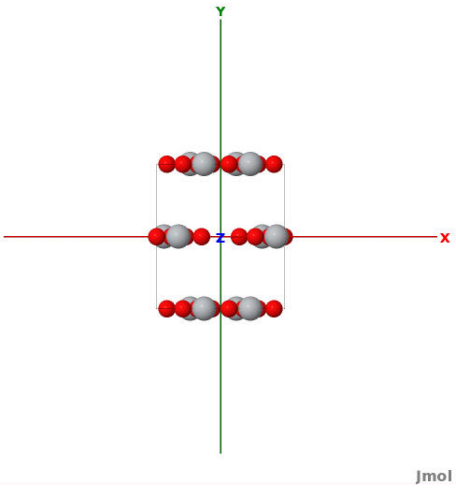

(c) Projection along c-axis

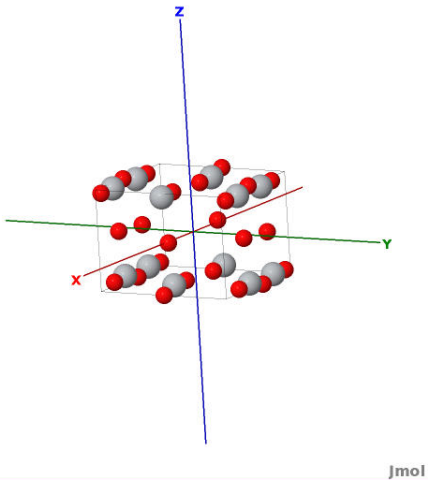

(d) Projection to the unit cell

Different projction of the beta phase of TiO_2 (gray atoms are titanium atoms and red ones are oxygens atoms) [70].

Attachment 5

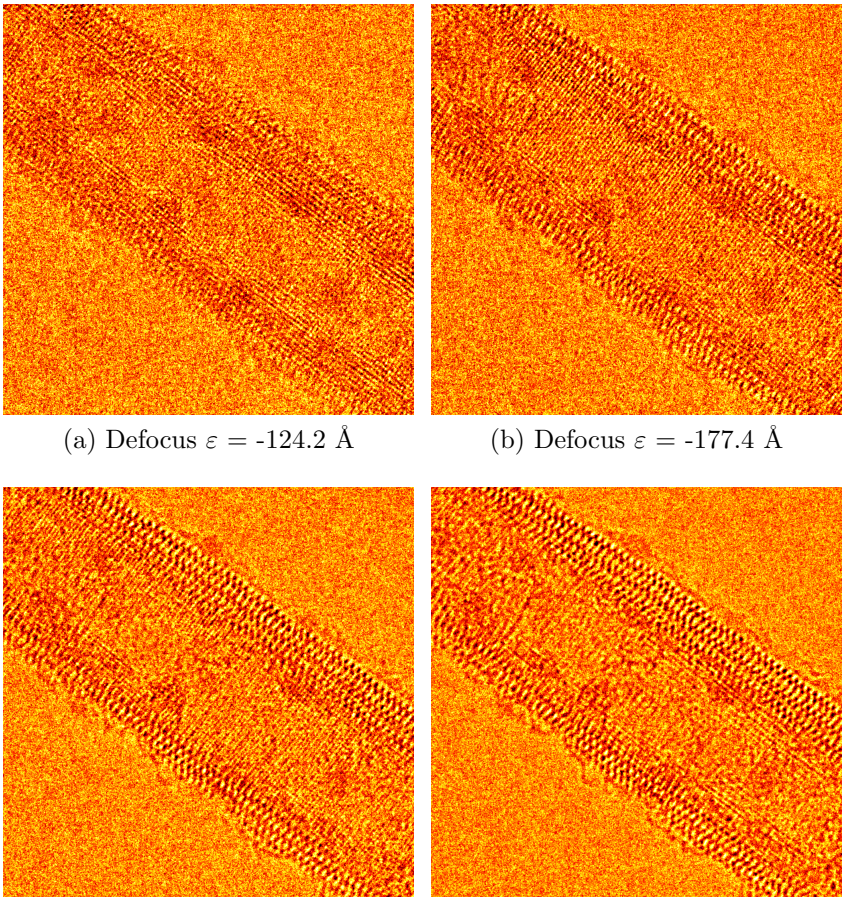

(a) Defocus ε = -124.2 Å

(b) Defocus ε = -177.4 Å

(c) Defocus ε = -230.6 Å

(d) Defocus ε = -283.8 Å

Through-focus series of HRTEM images of single nanotube.

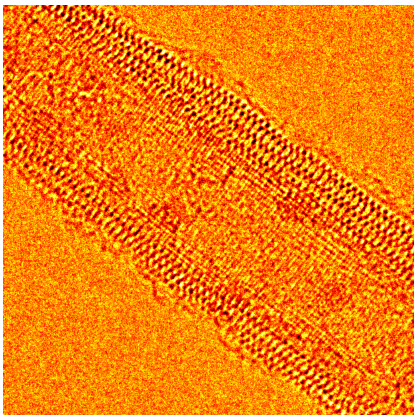

(e) Defocus ε = -337 Å

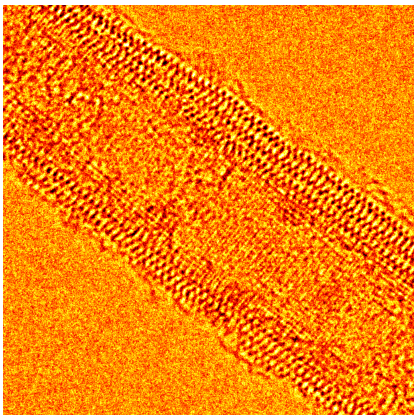

(f) Defocus ε = -390.2 Å

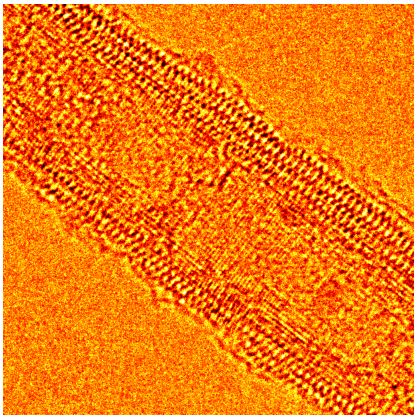

(g) Defocus ε = -443.4 Å

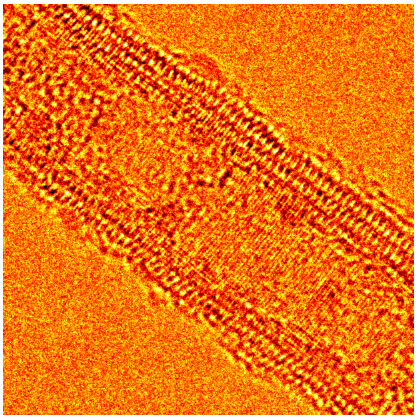

(h) Defocus ε = -496.6 Å

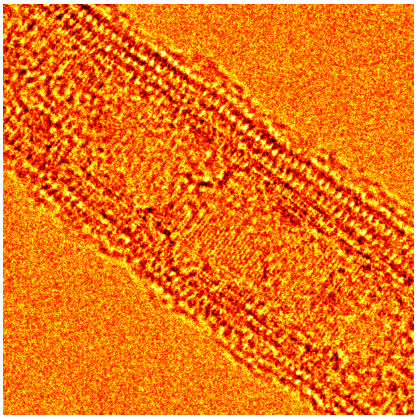

(i) Defocus ε = -549.8 Å

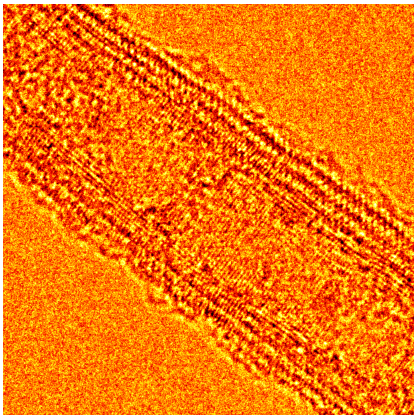

(j) Defocus ε = -603 Å

Through-focus series of HRTEM images of single nanotube.

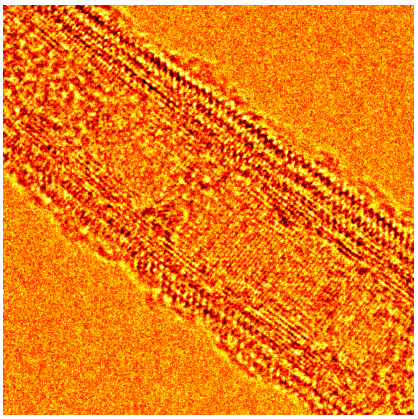

(k) Defocus ε = -656.2 Å

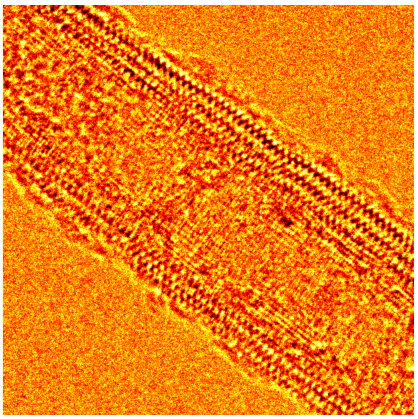

(l) Defocus ε = -709.4 Å

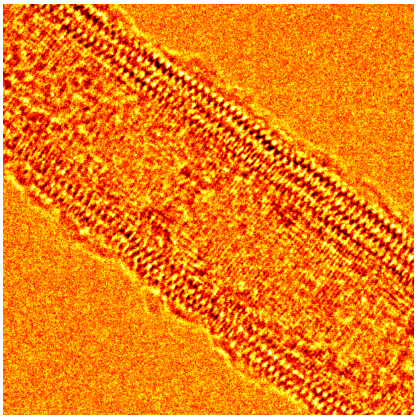

(m) Defocus ε = -762.6 Å

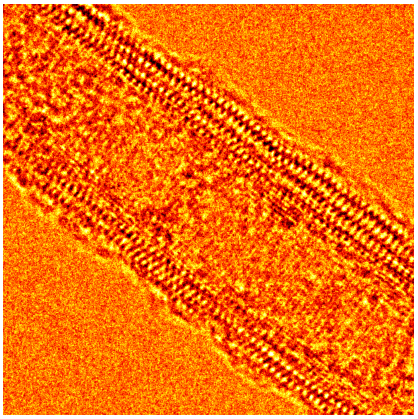

(n) Defocus ε = -815.8 Å

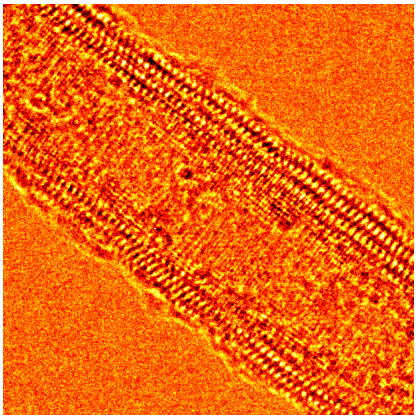

(o) Defocus ε = -869 Å

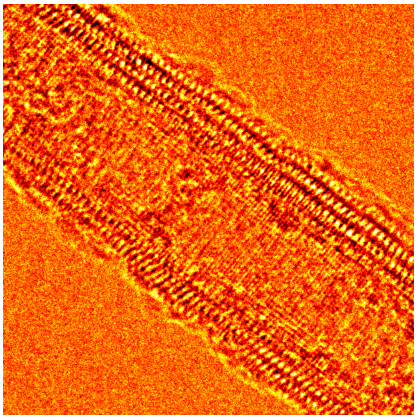

(p) Defocus ε = -922.2 Å

Through-focus series of HRTEM images of single nanotube.

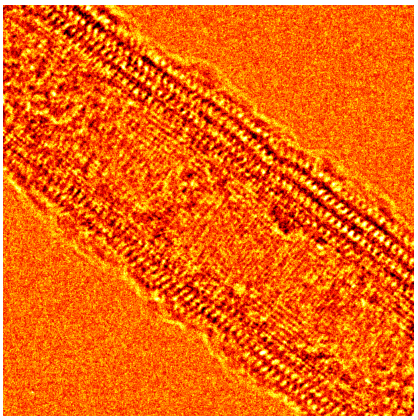

(q) Defocus ε = -975.4 Å

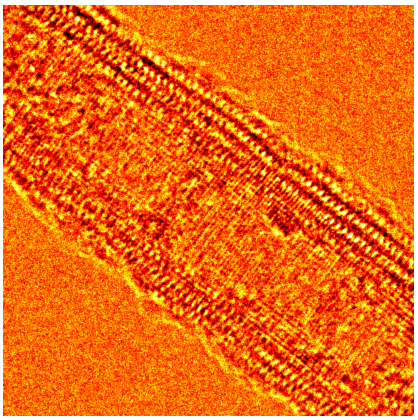

(r) Defocus ε = -1028.6 Å

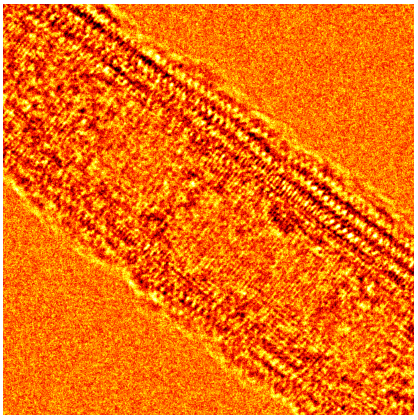

(s) Defocus ε = -1081.8 Å

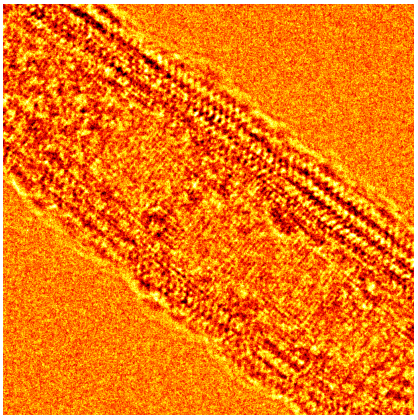

(t) Defocus ε = -1135 Å

Through-focus series of HRTEM images of single nanotube.